Ionosphere/Thermosphere/ Plasmasphere

Shigeto Watanabe
Hokkaido University

Solar Radiation

HINODE/XRT (0.6nm～20nm)

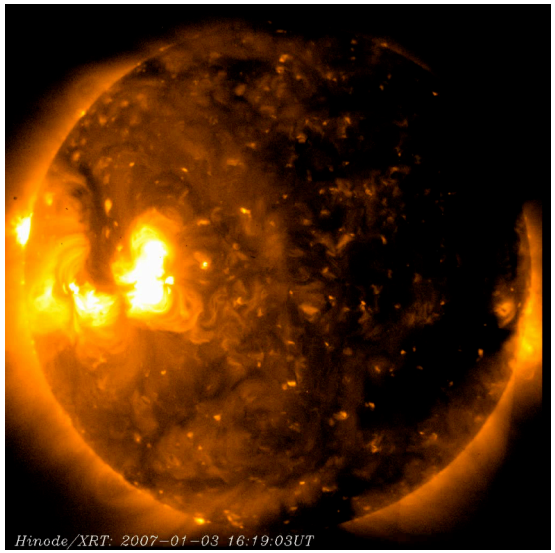

EUV: Extreme UltraViolet

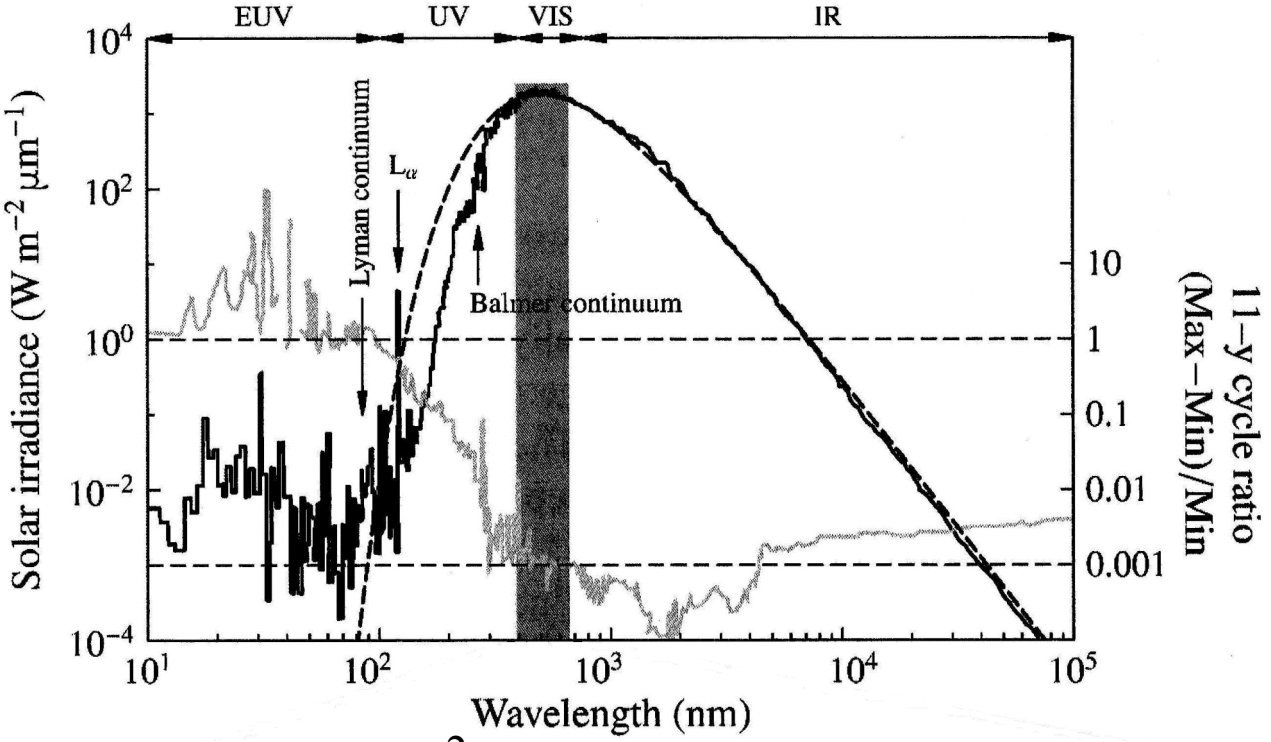

Planck's law

$$I(\lambda) = \frac{2hc^2}{\lambda^5} \frac{1}{e^{\frac{hc}{k\lambda T}} - 1}$$

Stefan–Boltzmann law

$$F = \int_0^\infty I(\lambda) d\lambda = \sigma T^4$$

$$C_s = 1.37 \mathrm{kW/m^2}$$

Solar Constant

Absorption of Solar Radiation

$$\Phi(\lambda, z) = \Phi(\lambda, \infty) e^{-\tau(\lambda, z, \chi)}$$

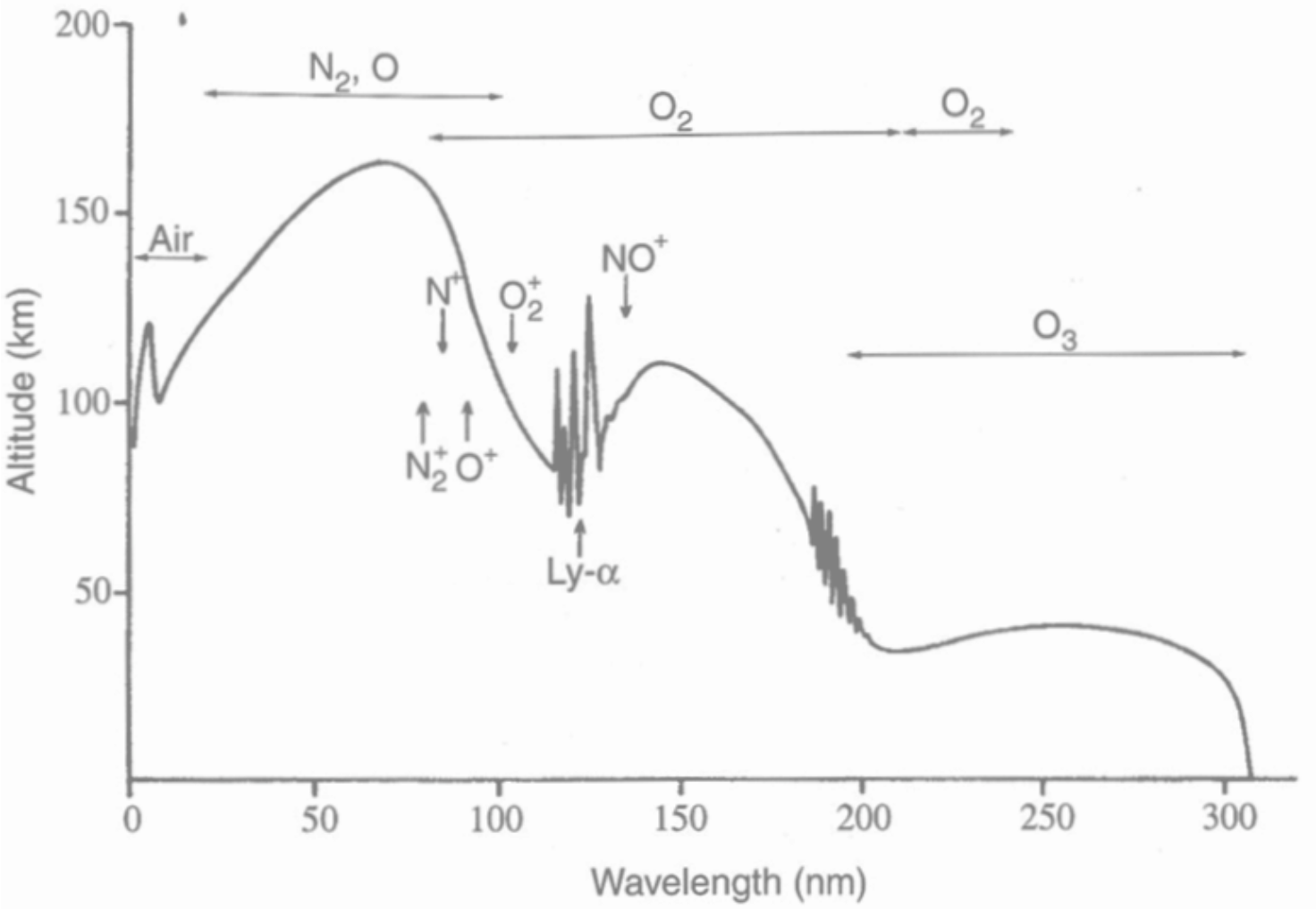

Photochemistry in the Upper Atmosphere

Photoionization by EUV

$$O + h\acute{\imath} \rightarrow O^+ + e$$

$$O_2 + h\acute{\imath} \rightarrow O_2^+ + e$$

$$N_2 + h\acute{\imath} \rightarrow N_2^+ + e$$

$$He + h\acute{\imath} \rightarrow He^+ + e$$

Radiative Recombination

$$O^+ + e \rightarrow O + h\acute{\imath}$$

$$He^+ + e \rightarrow He + h\acute{\imath}$$

$$H^+ + e \rightarrow H + h\acute{\imath}$$

Electron-Ion Recombination

$$NO^+ + e \rightarrow N + O$$

$$O_2^+ + e \rightarrow O + O$$

$$N_2^+ + e \rightarrow N + N$$

Ion-Molecule Reactions

$$O^+ + N_2 \rightarrow NO^+ + N$$

$$O^+ + O_2 \rightarrow O + O_2^+$$

$$O_2^+ + NO \rightarrow O_2 + NO^+$$

$$N_2^+ + O \rightarrow NO^+ + N$$

$$N_2^+ + O_2 \rightarrow N_2 + O_2^+$$

$$H^+ + O \rightarrow H + O^+$$

Ionosphere and Thermosphere

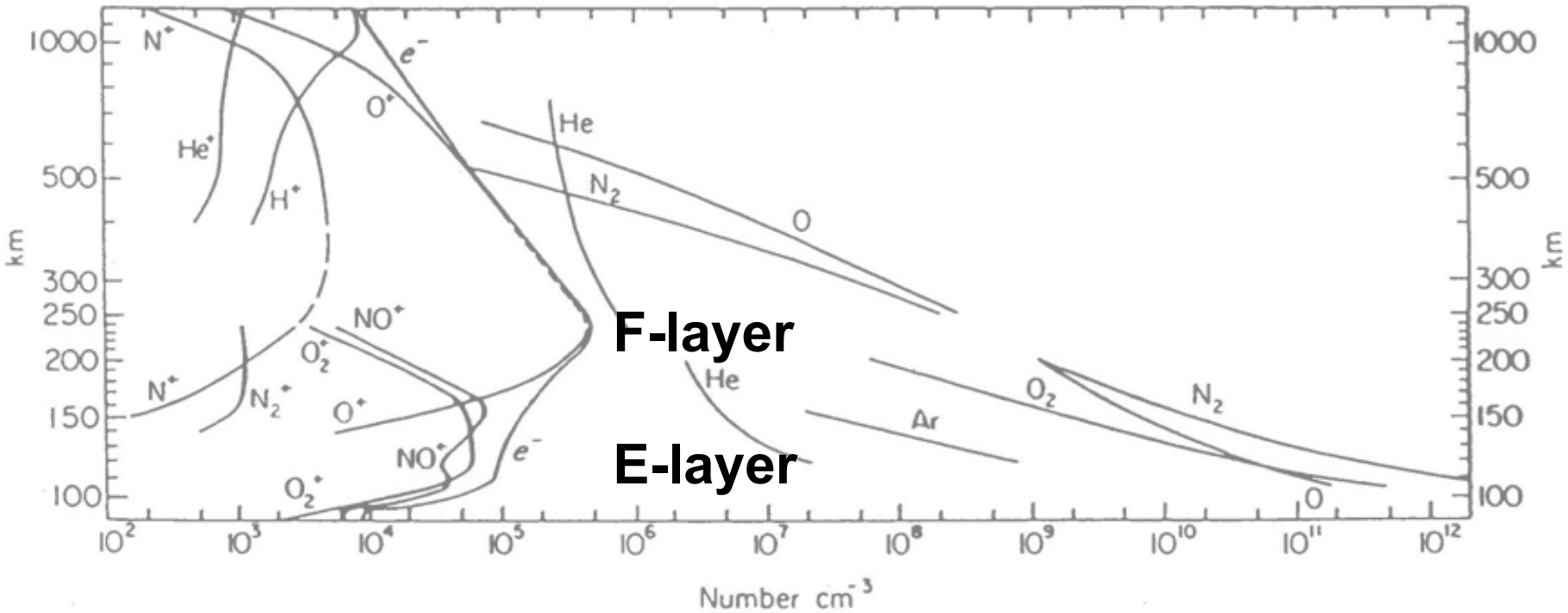

Ionosphere **Thermosphere**

***Ionization rate is $<10^{-4}$ in F-region.**

***Coupling between Atmosphere and Plasma is important for the dynamics and photochemistry in the ionosphere/thermosphere.**

Production of Photoelectron

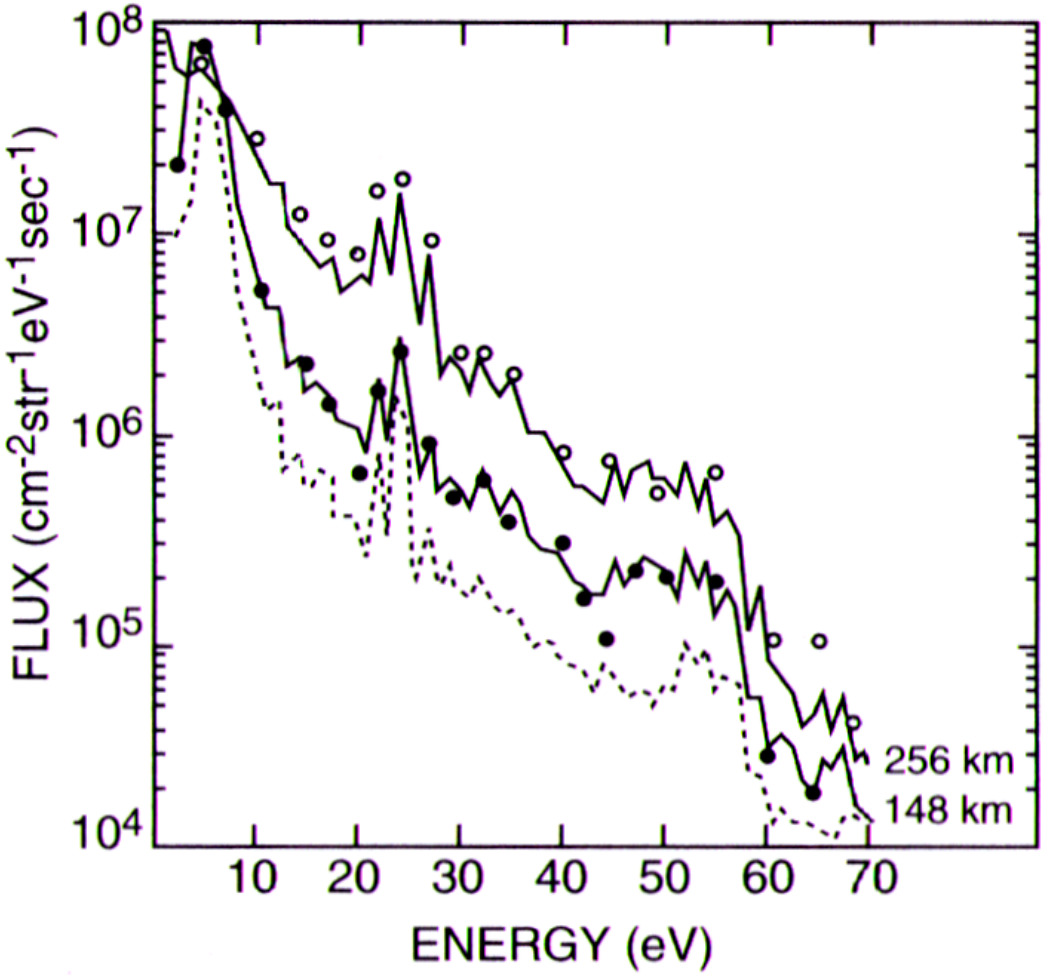

$$O + h\acute{\imath} \rightarrow O^+ + e$$

$$O_2 + h\acute{\imath} \rightarrow O_2^+ + e$$

$$N_2 + h\acute{\imath} \rightarrow N_2^+ + e$$

$$He + h\acute{\imath} \rightarrow He^+ + e$$

Temperatures in the Upper Atmosphere

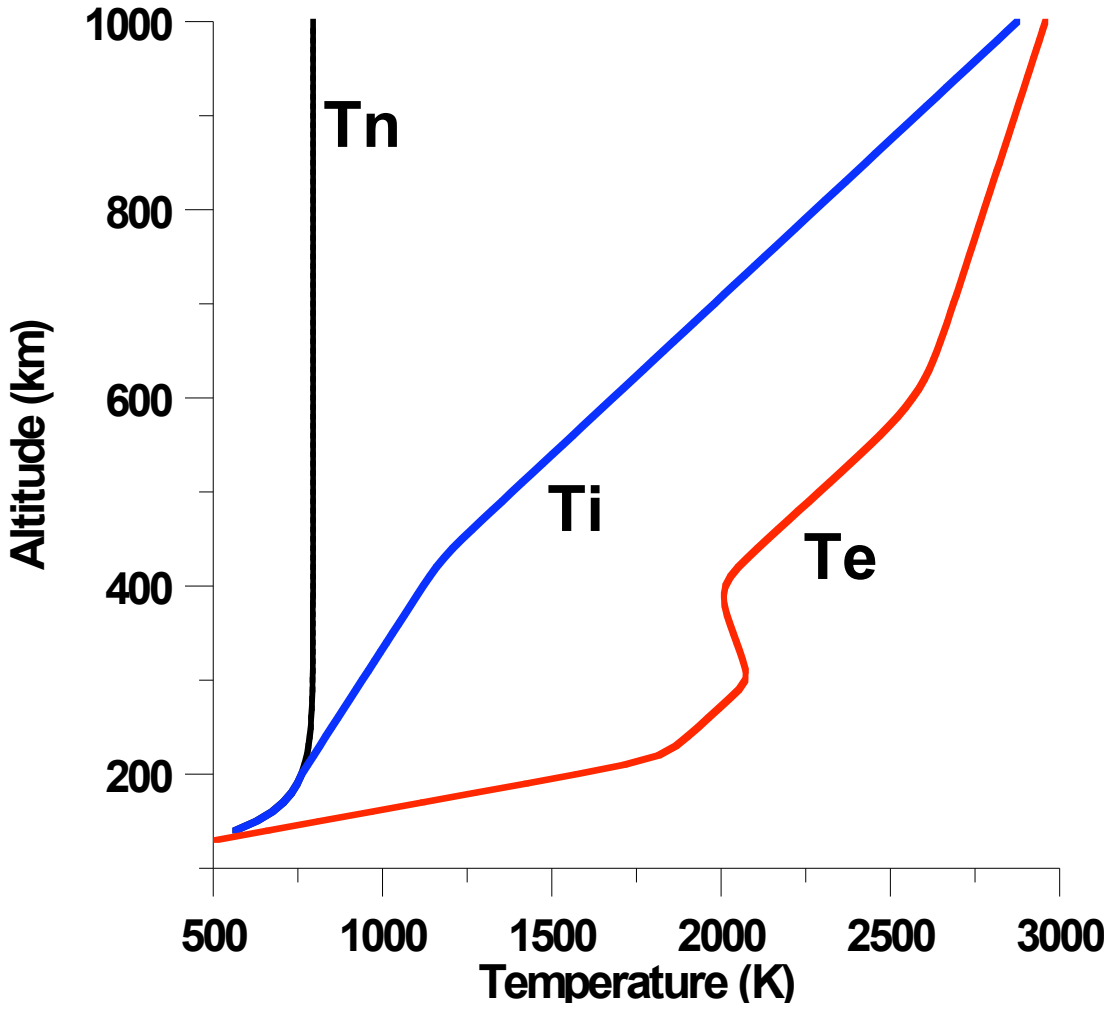

IRI 2005/8/29/1.5UT/43Lat/140Lon

Energy Flow

Photoelectron

↓

Ambient Electron

↓

Ion

↓

Neutral Atmosphere

Planetary Ionospheres

Venus

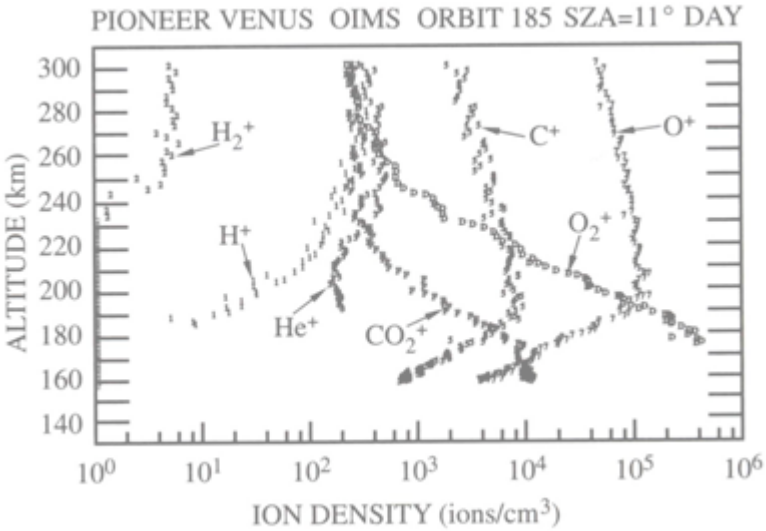

Mars

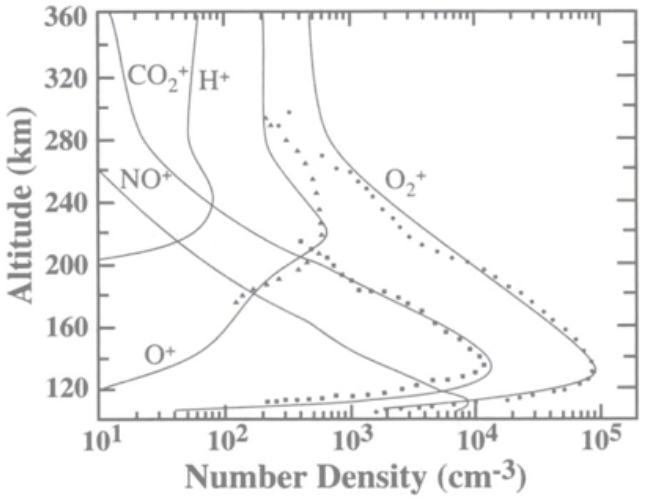

Jupiter

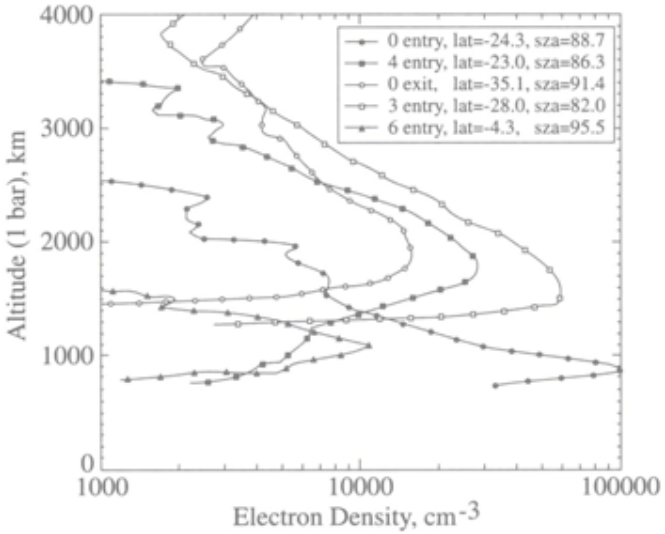

Io

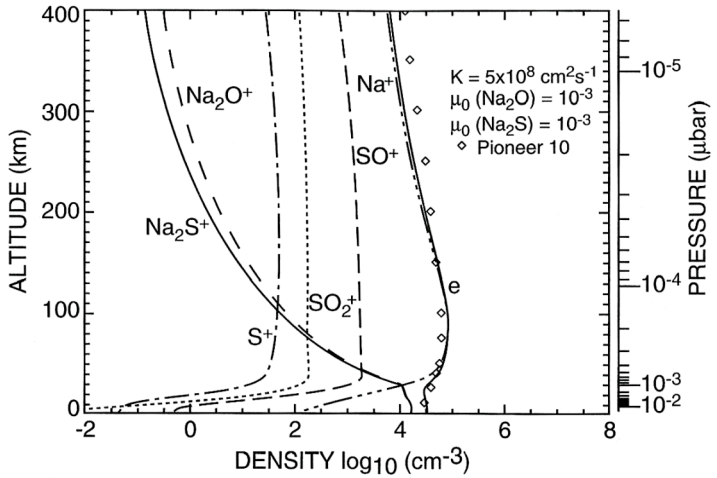

Ionosphere/Thermosphere/Plasmasphere

1. 磁気圏プラズマ供給源としての電離層
2. 熱圏嵐と電離圏嵐
3. プラズマ不安定

Plasmasphere

The Earth's plasmasphere is a torus of cold (~1eV) and dense (~$10^3 cm^{-3}$) plasma in the region of the inner magnetosphere.

H^+ is the principal ion with ~20% He^+

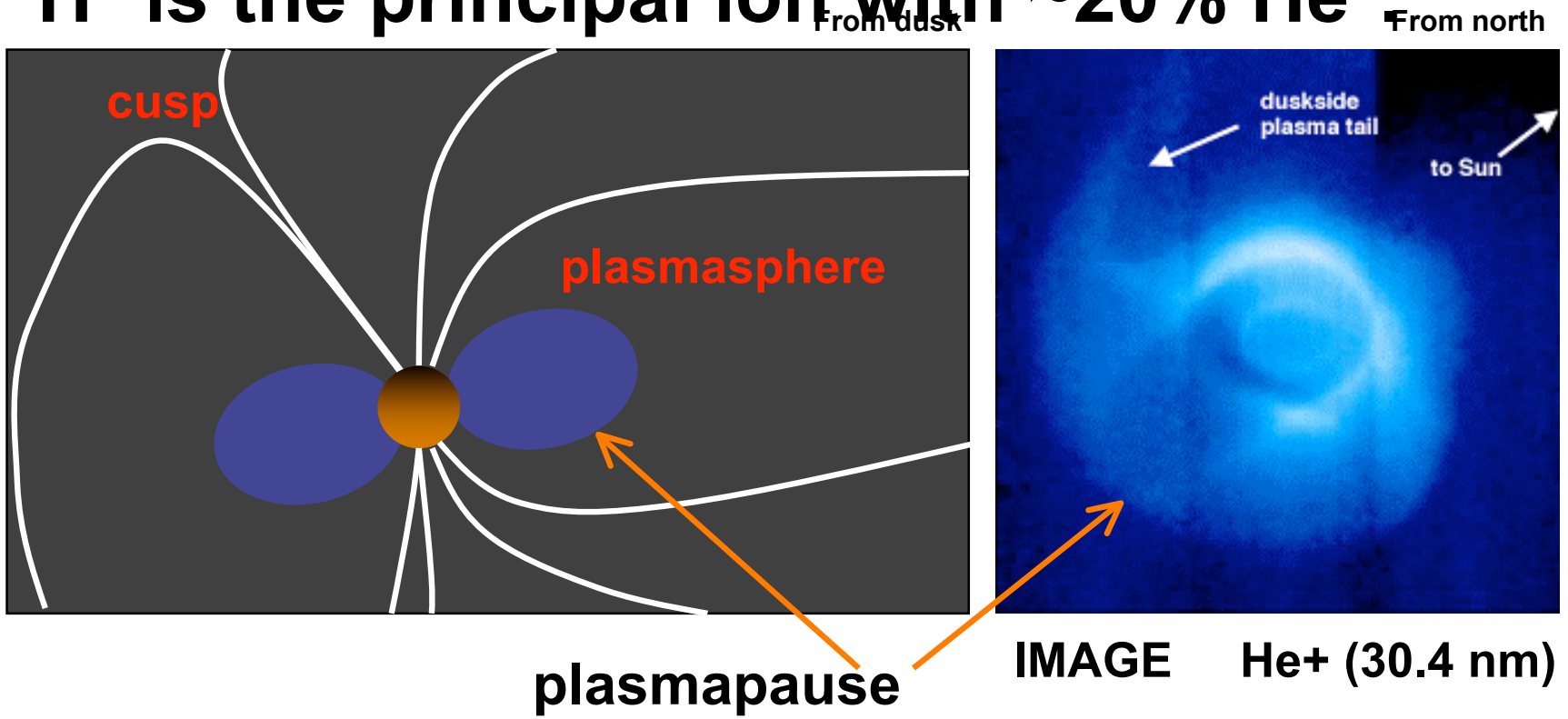

Magnetospheric Convection

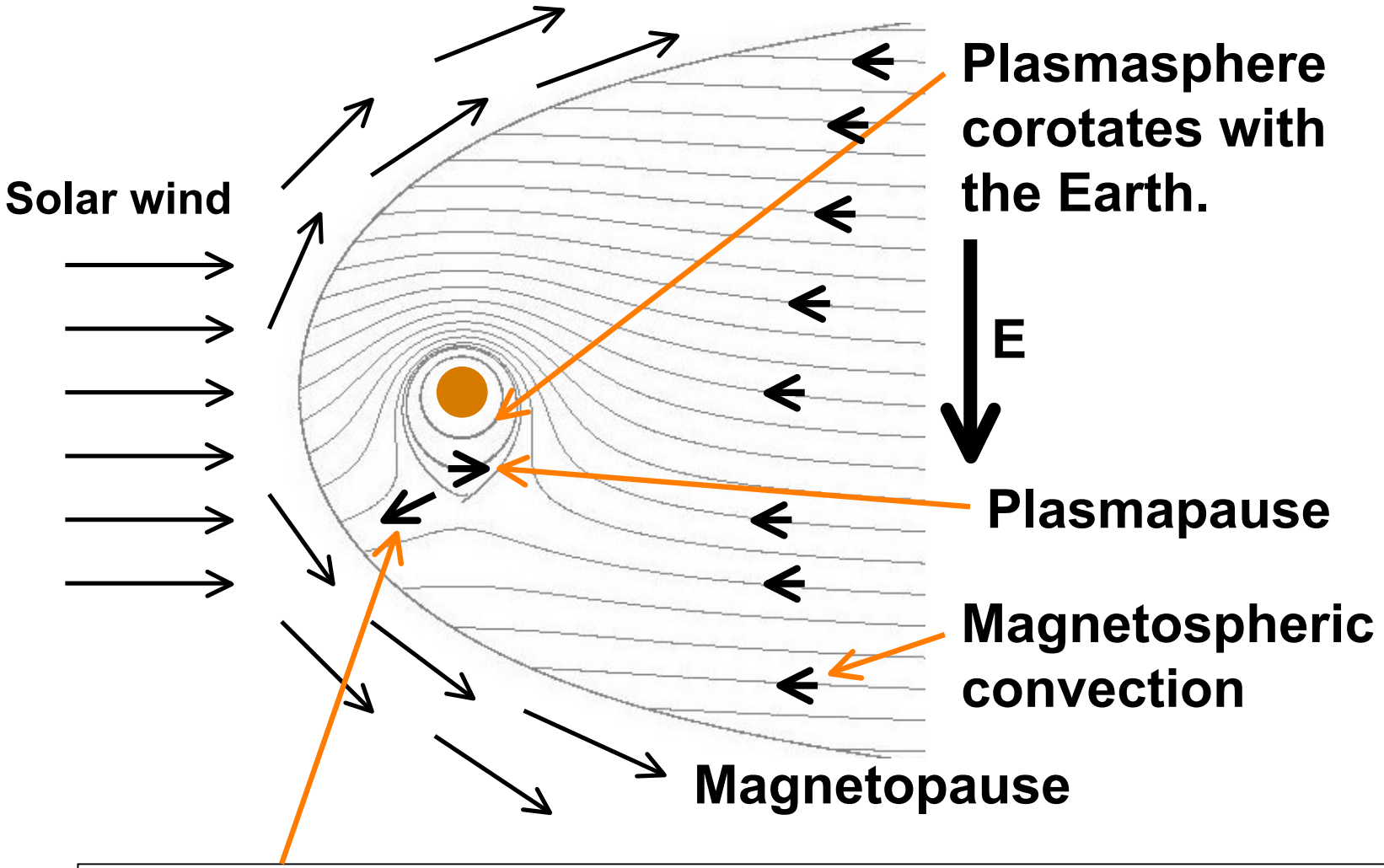

Plasmaspheric erosion (plasma tail) is the result of enhanced magnetospheric convection.

Plasmapause

Corcuff et al., 1972

Ne (cm^{-3})

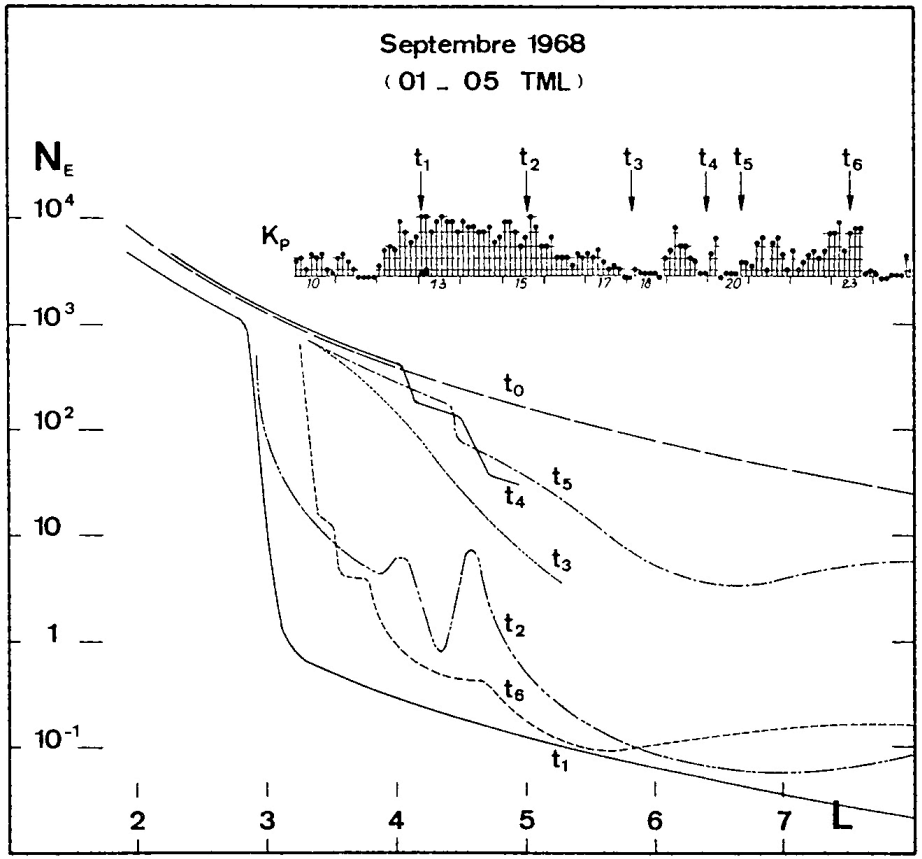

Plasmasphere Plasmapause

Carpenter and Park, 1973

$$L_{pp} = 5.7 - 0.47K_p$$

The location of the plasmapause depends on the magnetospheric disturbance.

Wave-like irregularity in the plasmapause results from transient, localized processes associated with substorms.

Plasma is supplied continuously from ionosphere. (Refilling)

Momentum Equation in Ionosphere

Momentum Equation for Ion and Electron

$$\rho_i \frac{\partial \mathbf{v}_{//i}}{\partial t} + \rho_i \left(\mathbf{v}_{//i} \cdot \nabla_{//}\right)\mathbf{v}_{//i} = -\nabla_{//} p_i + e n_i \mathbf{E}_{//} - \rho_i \mathbf{g}_{//} - \rho_i \nu_{ie}\left(\mathbf{v}_{//i} - \mathbf{v}_{//e}\right)$$

Charge Neutrality **Ambipolar Electric Field**

$$m_e << m_i, \qquad \left|n_i - n_e\right| << n_i, n_e, \qquad \mathbf{E}_{//} = -\frac{\nabla_{//} p_e}{e n_e}$$

$$\rho_i \frac{\partial \mathbf{V}_{//}}{\partial t} + \rho_i \left(\mathbf{V}_{//} \cdot \nabla_{//}\right)\mathbf{V}_{//} = -\nabla_{//} p - \rho_i \mathbf{g}_{//}, \qquad p = p_i + p_e$$

Force along Open Magnetic Field Line
or Closed Magnetic Field Line during Refilling.

- **Pressure Gradient**
- **Ambipolar Electric Field** ←

Modeling of Topside Ionosphere

Boundary Condition: H+ density at 3000km altitude.

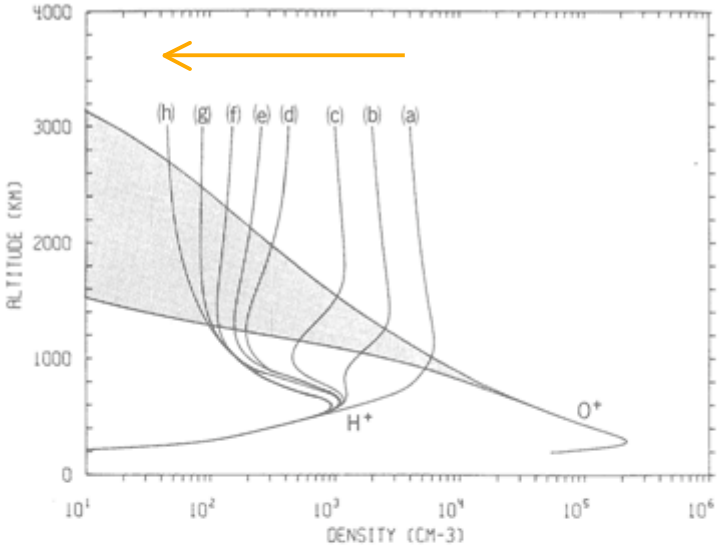

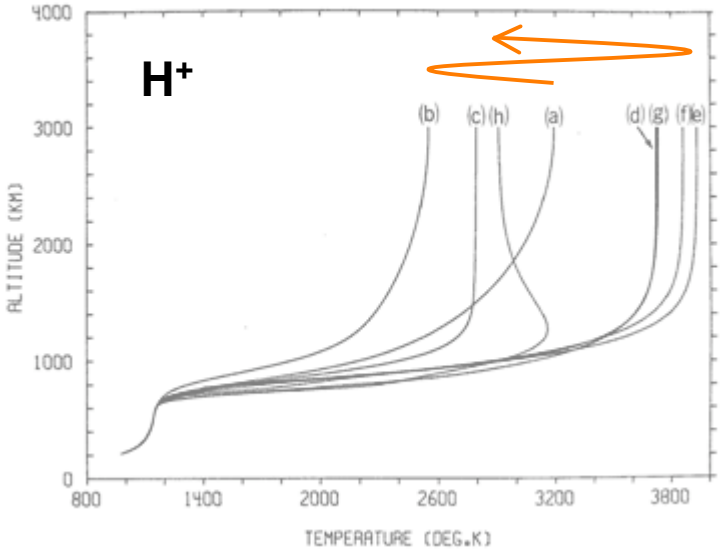

Collisional Coupling
H+ - O+
H+ - e

Te: 1000k at 200km
4650k at 3000km

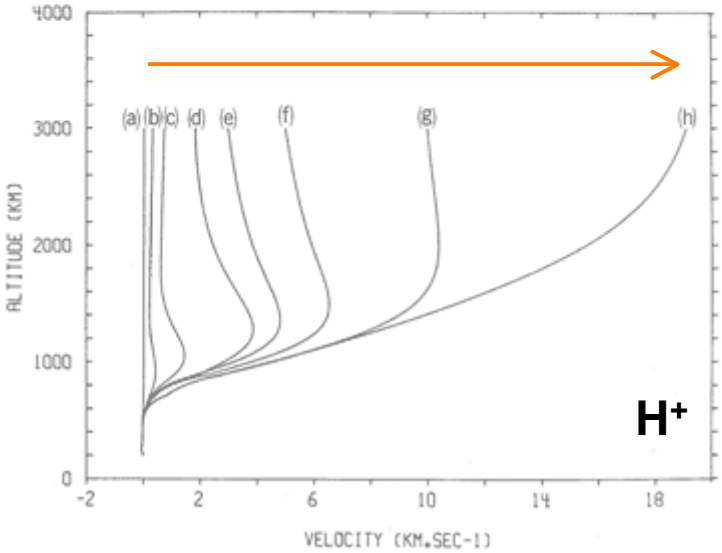

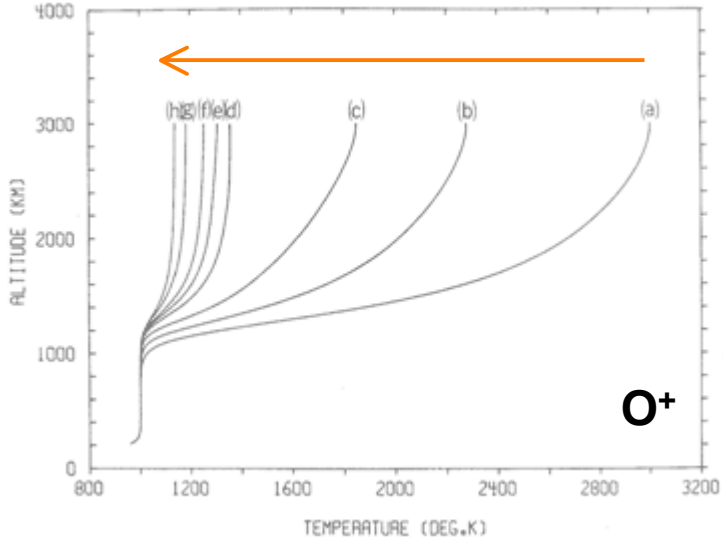

Raitt et al., 1975

Polar Wind

Axford [1968] pointed out that the lighter ions must escape from the earth by the flux of escaping photo-electrons with energies greater than 2.4 eV, and suggested the ion escape speed of ~10 km/sec.

This phenomenon is called 'Polar Wind'.

The polar wind is important as a source of magnetospheric plasma [Shelley et al., 1982; Moore et al., 1986; Chappell et al., 1987].

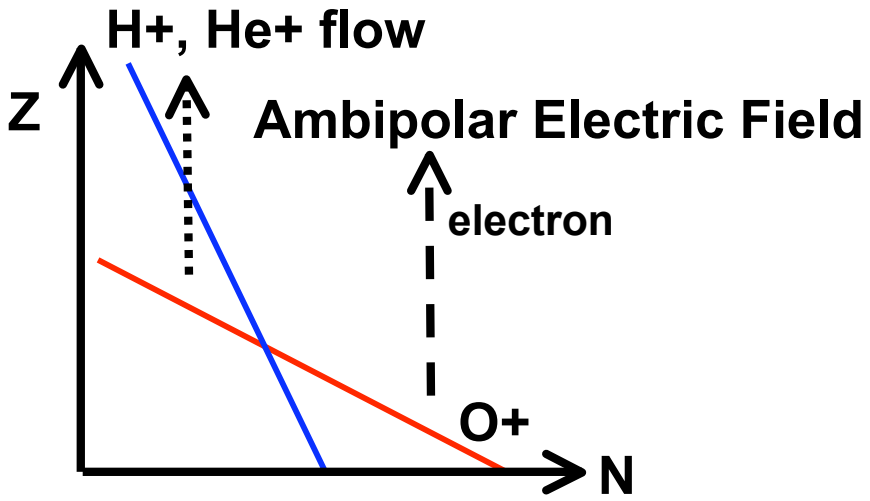

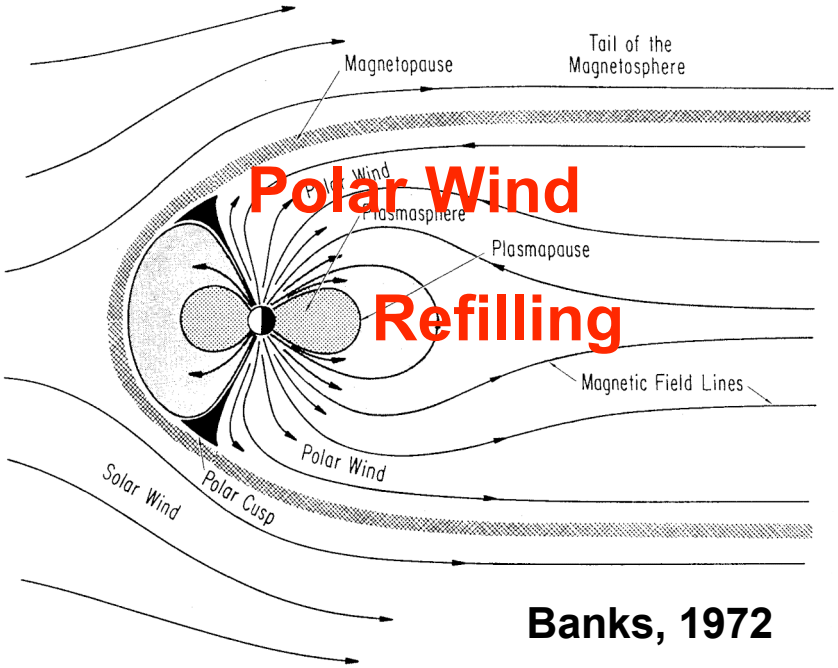

Banks, 1972

Thermal Ion Outflow

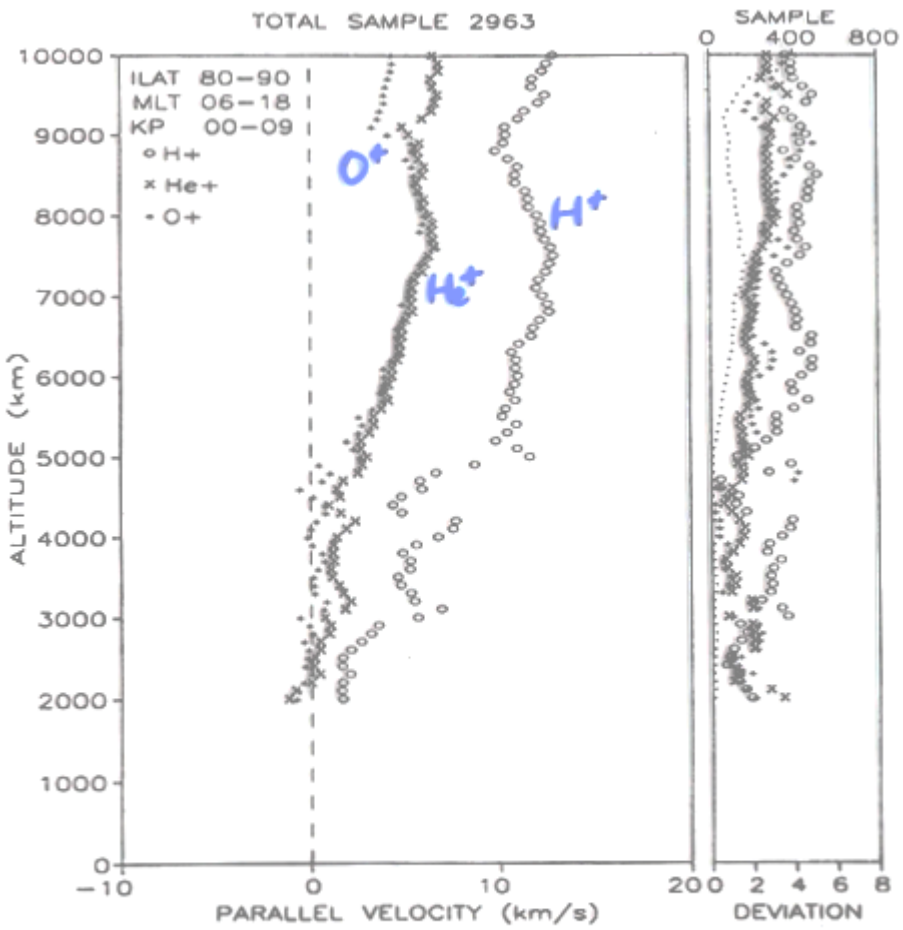

Fig. 4. Parallel ion velocity of the polar wind in the dayside (06-18 MLT) as a function of altitude, averaged over all *Kp* levels and all invariant latitudes above 80°. See Figure 3 caption for explanation.

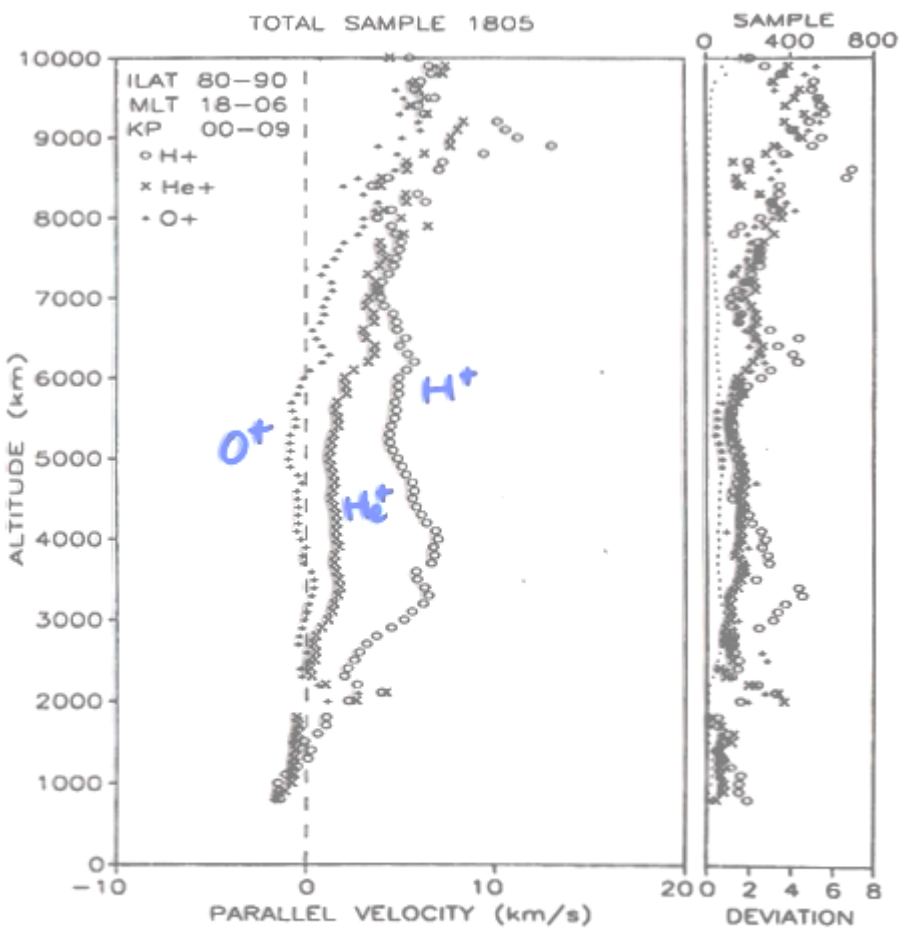

Fig. 5. Parallel ion velocity of the polar wind in the nightside (18-06 MLT) as a function of altitude, averaged over all *Kp* levels and all invariant latitudes above 80°. See Figure 3 caption for explanation.

Akebono/SMS

Near magnetic pole,
all ionospheric ions are flowing to Magnetosphere.

Thermal Ion Heating

O+
H+
e
E
B
n
B
j

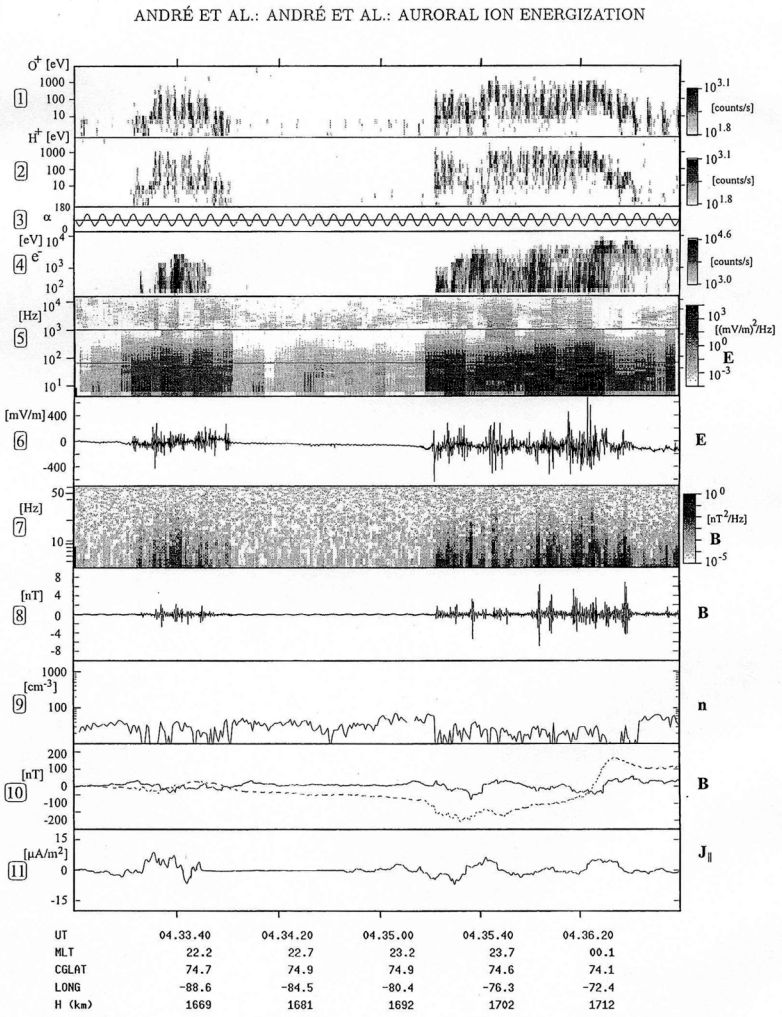

Figure 1. Freja data from orbit 5972 (January 1, 1994) where the satellite passed an ion heating region near midnight (event 1). Panel 1 and 2 show the count rates of O^+ and H^+, while panel 3 displays the corresponding pitch angles. Panel 4 displays count rates of downgoing electrons. Panel 5 shows the electric field spectral density up to about 10 kHz, while panel 6 displays a time series of the perpendicular electric field. Panel 7 shows the magnetic field spectral density up to 60 Hz, while panel 8 displays a time series of the magnetic field. Panel 9 shows an estimate of the density. Panel 10 displays magnetic perturbations in the geographic northward (solid) and eastward (dashed) directions. Panel 11 contains the field-aligned current intensity calculated using the magnetic perturbations shown in Panel 10. A positive field-aligned intensity represents an upward current. Transversely heated O^+ ions can be seen in panel 1 between 0433:30 and 0433:50 UT and also between 0435:20 and 0436:30 UT. There is a good correlation between waves in panels 5 and 7 and ion energization in panel 1, as is further discussed in the text. See also Figures 2 and 3.

In Cusp/Aurora regions, ions are heated perpendicular to the local magnetic field line.

This is called TAI. (Transversely Accelerated Ion)

There is good correlation between TAI and Electric/Magnetic field variations. (Low frequency waves)

Freja

Transversely Accelerated Ion

Akebono (EXOS-D)

Thermal H+

O+

Energetic Ele.

Ion

Electric Field

Magnetic Field

ELF wave E

B

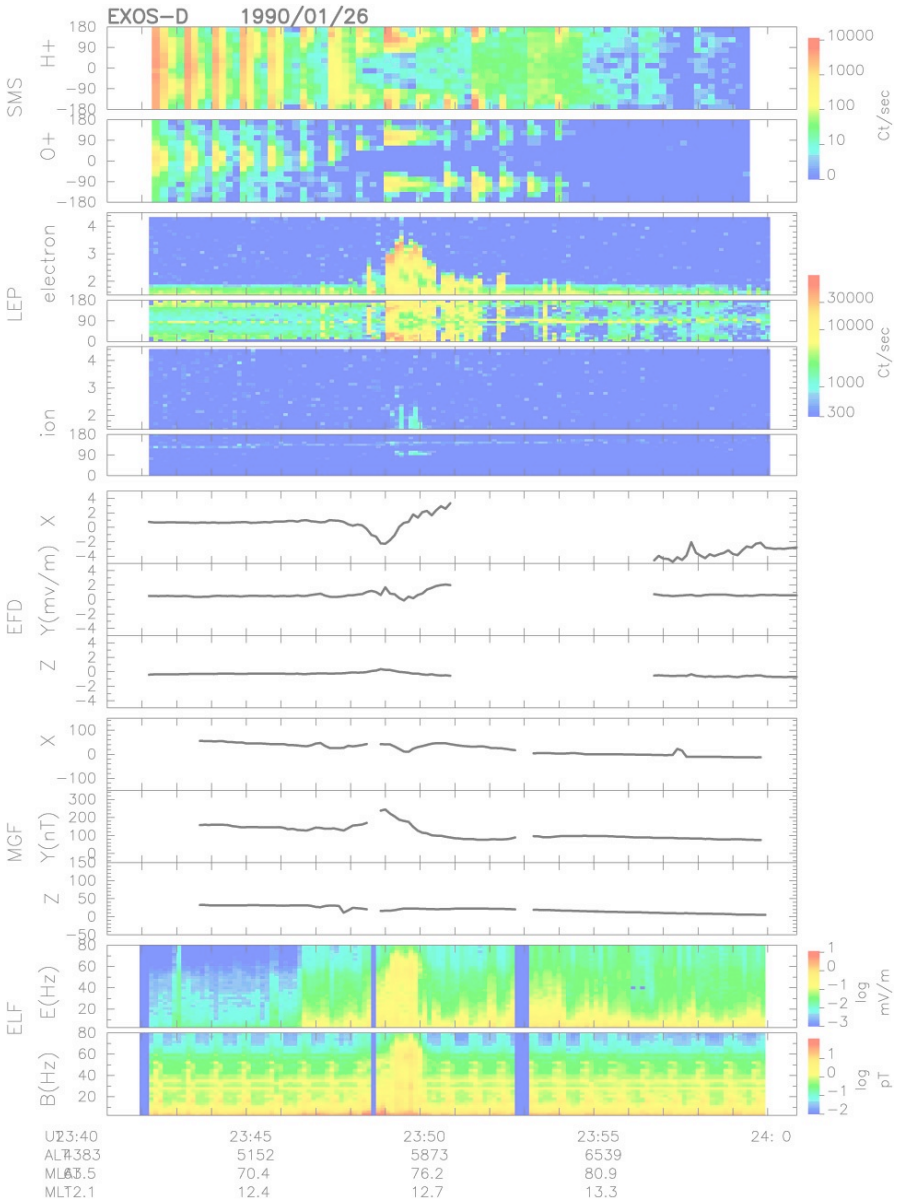

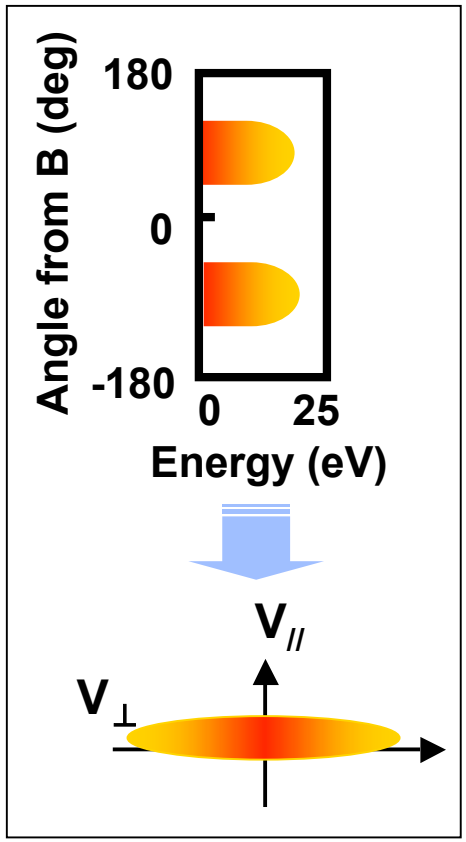

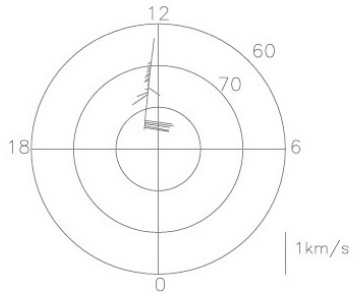

Outflow and Plasma wave

Akebono (EXOS-D)

Kasahara et al., 2000

Broadband Noise

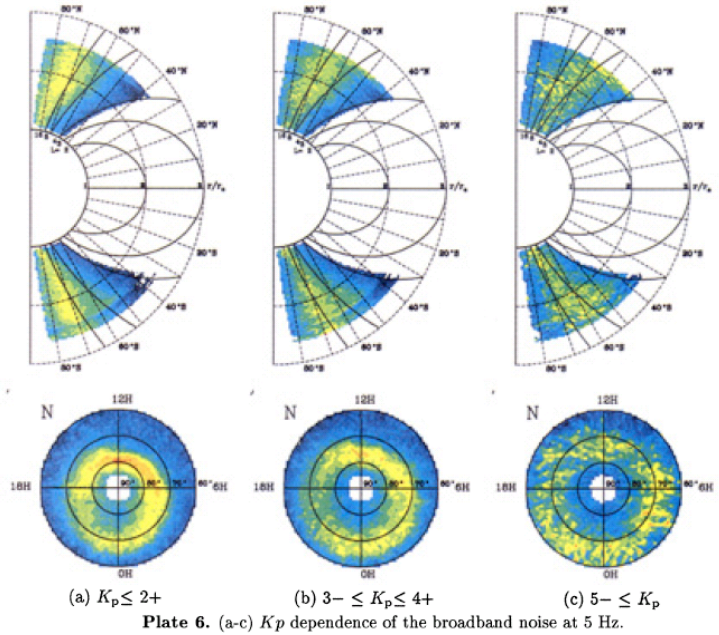

(a) $K_p \leq 2+$ (b) $3- \leq K_p \leq 4+$ (c) $5- \leq K_p$

Plate 6. (a-c) *Kp* dependence of the broadband noise at 5 Hz.

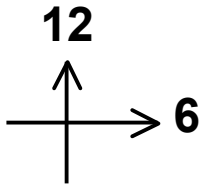

Velocity

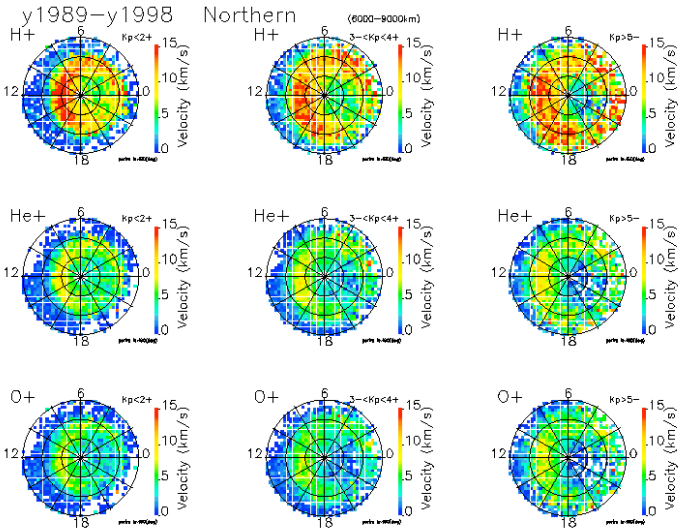

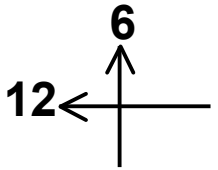

Kp <2+ 3- ~ 4+ >5-

Transversely Acceleration

●Acceleration by Cyclotron Resonance

Ion Motion

$$m\frac{d\mathbf{v}_{//}}{dt} = -\mu\frac{\partial \mathbf{B}}{\partial s} - \frac{GMm}{r^3}\hat{\mathbf{s}}$$

Lorentz force

Magnetic Moment (conserved)

$$\mu = \frac{m\mathbf{v}_{\perp 0}^2}{2\mathbf{B}_0}$$

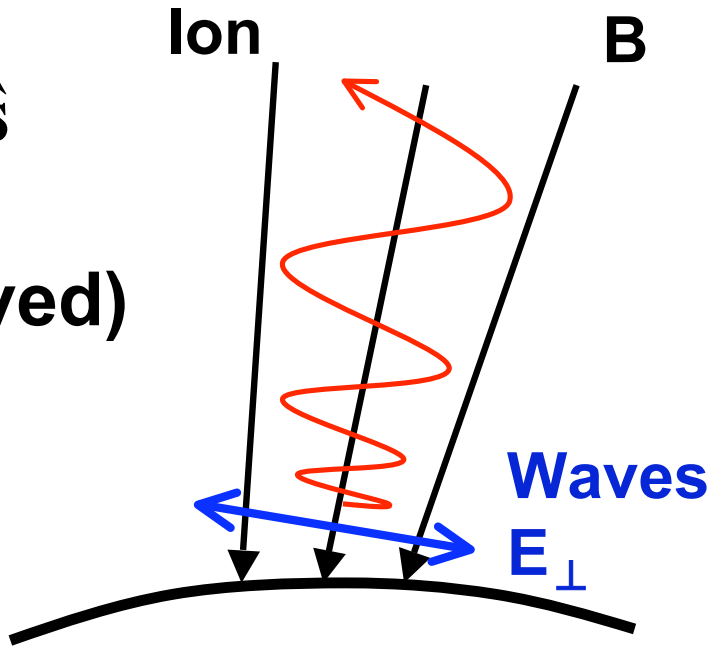

Ion Energy

$$\frac{d}{ds}\left(\frac{1}{2}m\mathbf{v}_{//}^2 + \mu\mathbf{B} + GMm\left(\frac{1}{r_0} - \frac{1}{r}\right)\right) = 0$$

Heating Wall

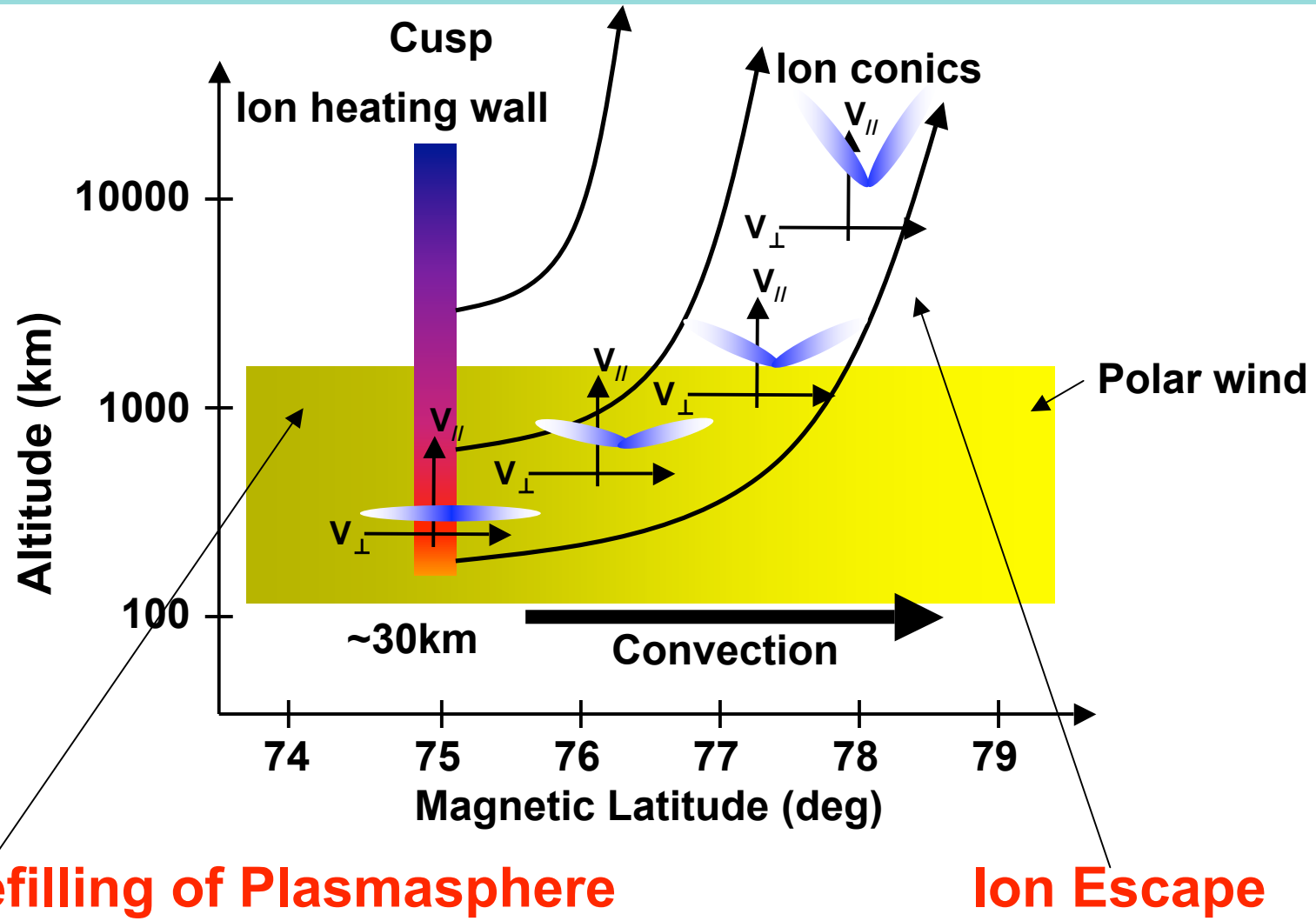

Correlation between Transversely Accelerated Ion and Broadband Extremely Low Frequency (BBELF) Turbulence.

Molecular Ion Heating

Akebono (EXOS-D)

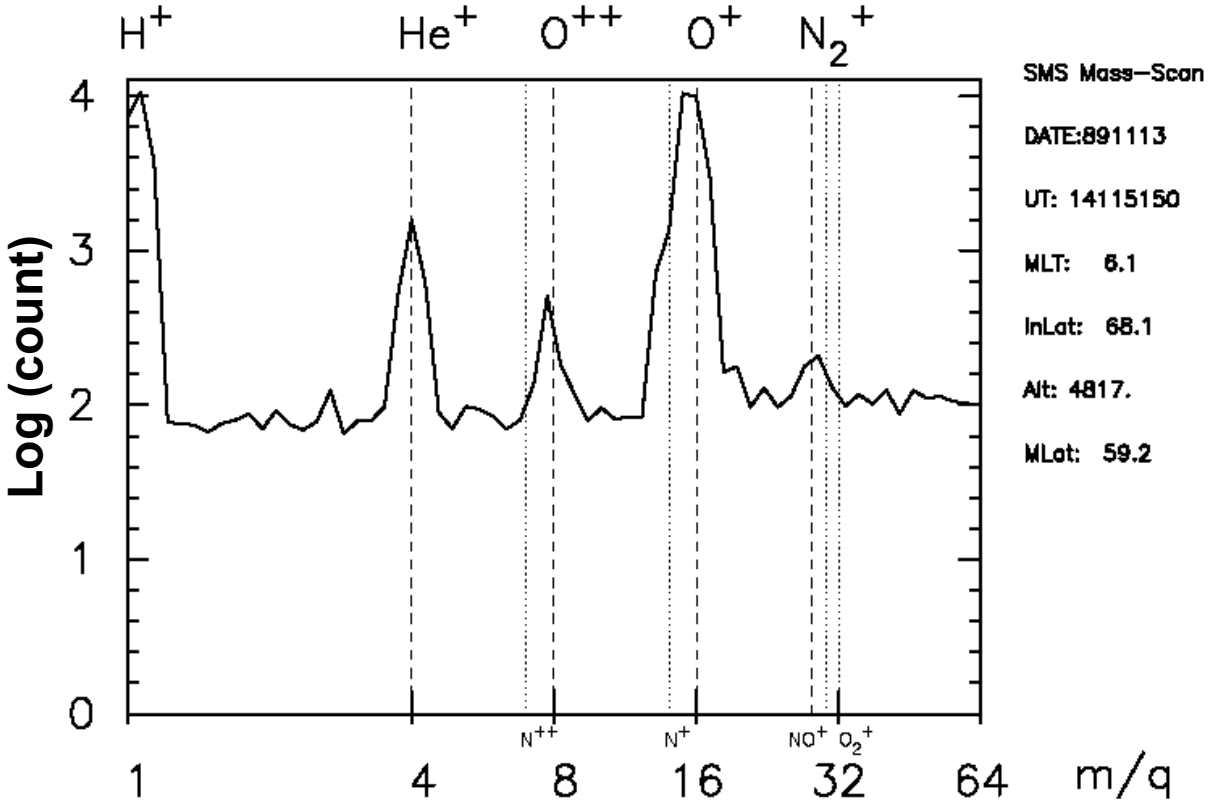

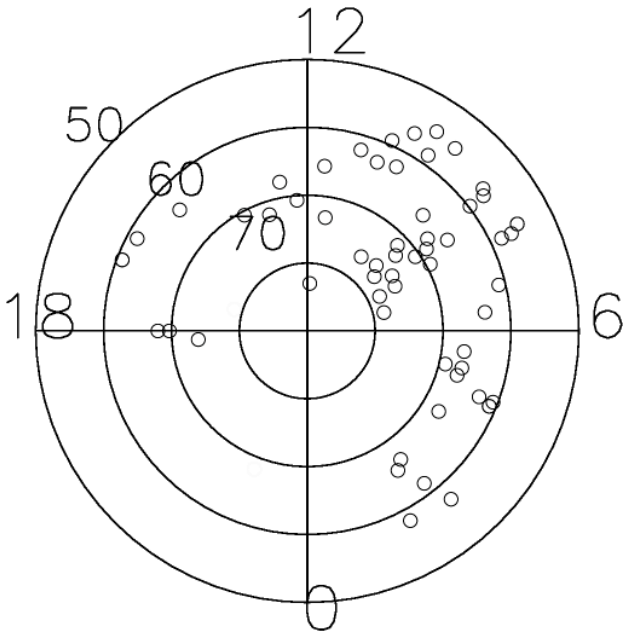

N_2^+ Occurrence

In the polar ionosphere, all ions are heated and flow to the magnetosphere.

Oxygen Ion in Magnetosphere

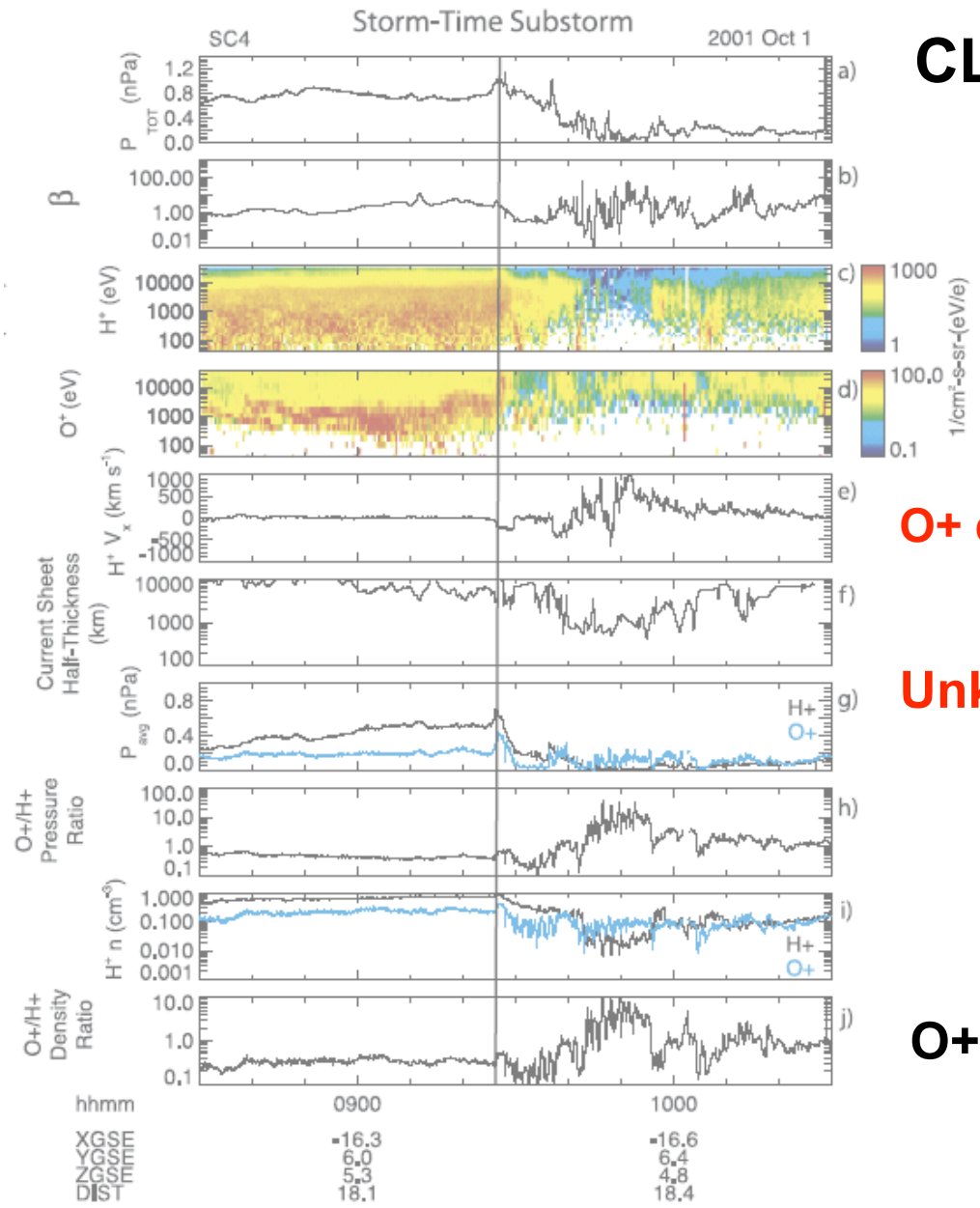

CLUSTER

O+ in plasma sheet.

O+ energy >10keV

larger than TAI energy

Unknown acceleration process!

O+ density is larger than H+.

Kistler et al., 2006

Ion Flux from Ion Outflow (Empirical Model)

Escape Flux at 6000 km altitude in the northern hemisphere

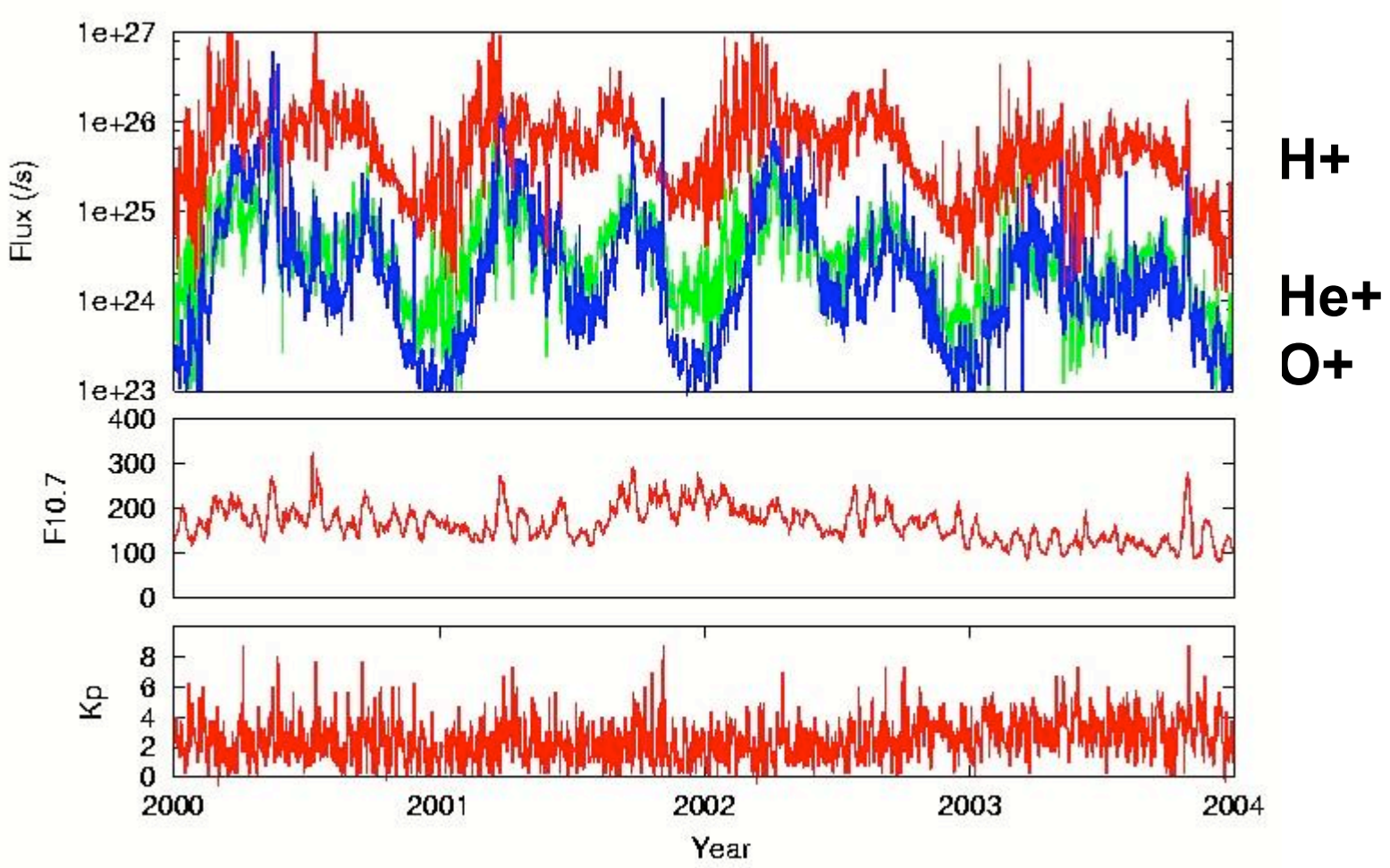

Mass Loss from Topside Polar Ionosphere

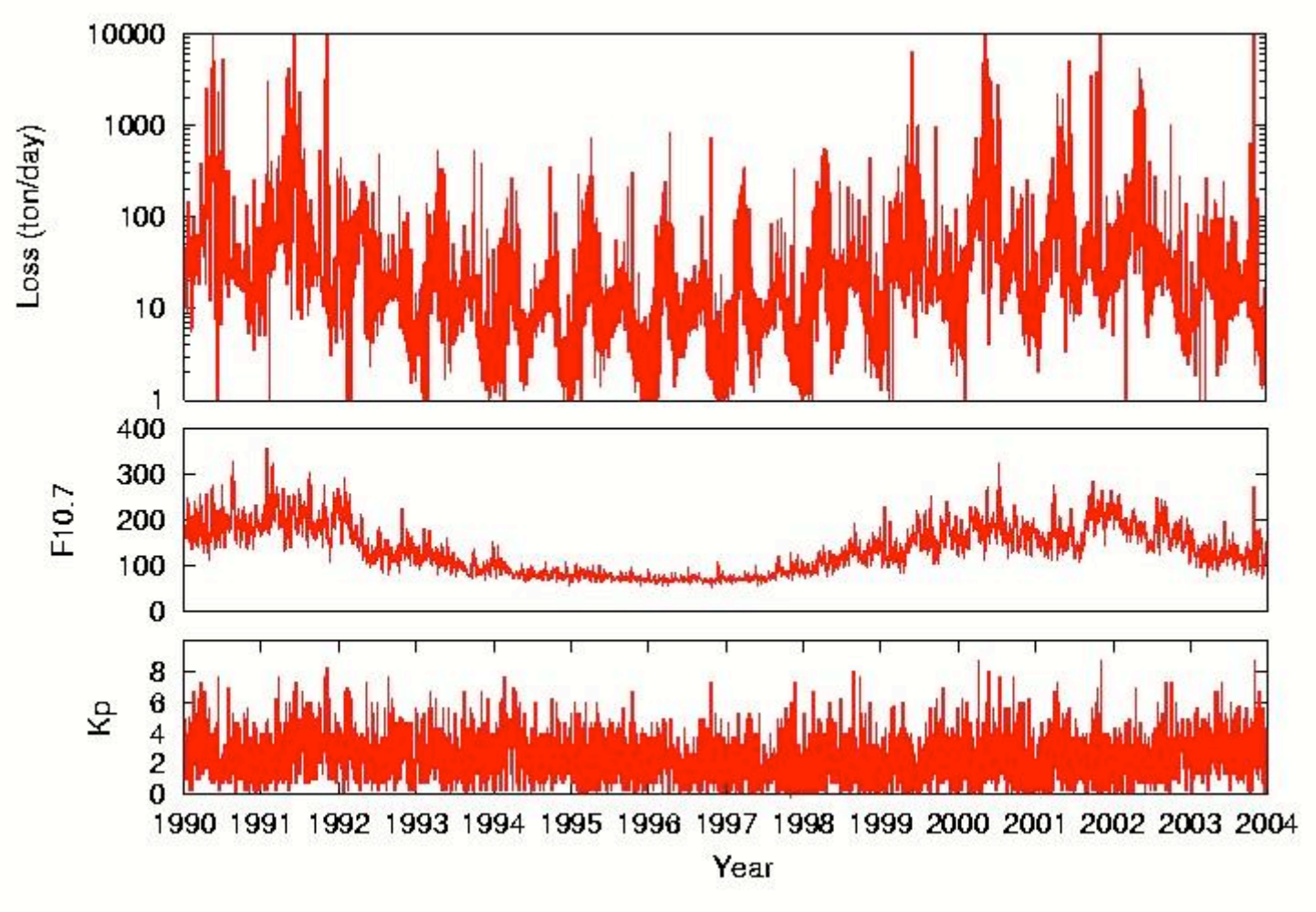

Total Oxygen Mass in Thermosphere

$$M_t = 4\pi r^2 m_O n_O H = 3\times 10^7 \, ton$$

Ionosphere/Thermosphere/Plasmasphere

1. 磁気圏プラズマ供給源としての電離層
2. 熱圏嵐と電離圏嵐
3. プラズマ不安定

Heating/Loss in Thermosphere

- **Heating**
  - **Dissociation**
    - $O_2 + h\nu \rightarrow O + O$, $N_2 + h\nu \rightarrow N + N$, …
  - **Dissociative ionization**
    - $N_2 + h\nu \rightarrow N^{+*} + N + e$, …
  - **Ionization**
    - $O + h\nu(30.4nm) \rightarrow O^{+} + e + 27eV$, …
  - **Excitation**
    - $O + h\nu \rightarrow O^{*}$, …
  - **Excitation by Auroral Particle, Joule Heating**

- **Heat Loss**
  - **Radiation cooling**
    - **NO, CO2**
  - **Molecular heating conduction**

Atoms/Molecules in Thermosphere

F10.7=250

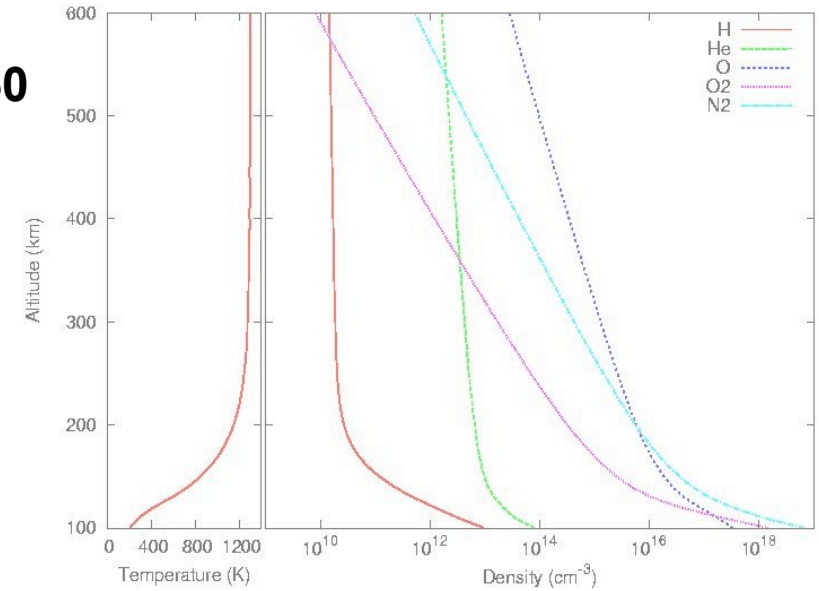

F10.7=70

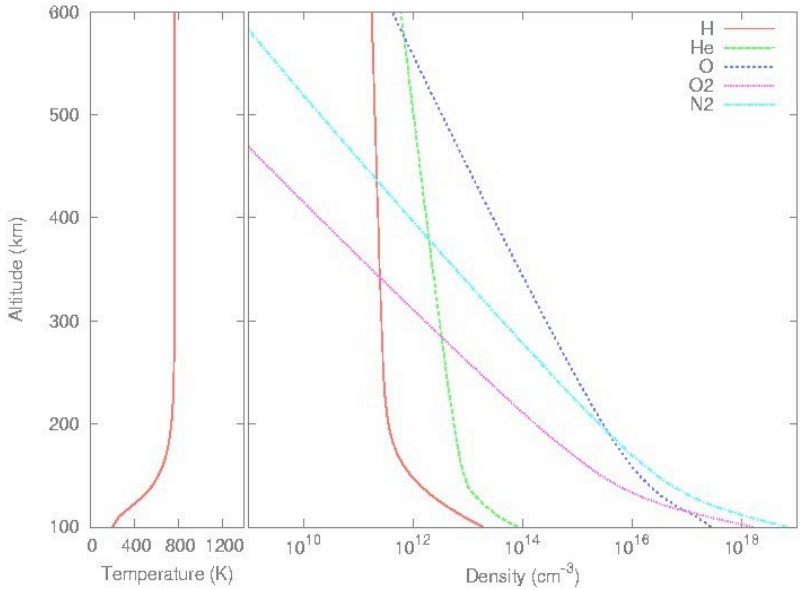

外圏（Exosphere）

$\lambda > H$

熱圏界面（Thermopause）

$\lambda = H$

熱圏（Thermosphere）

$\lambda < H$

Winds in Thermosphere

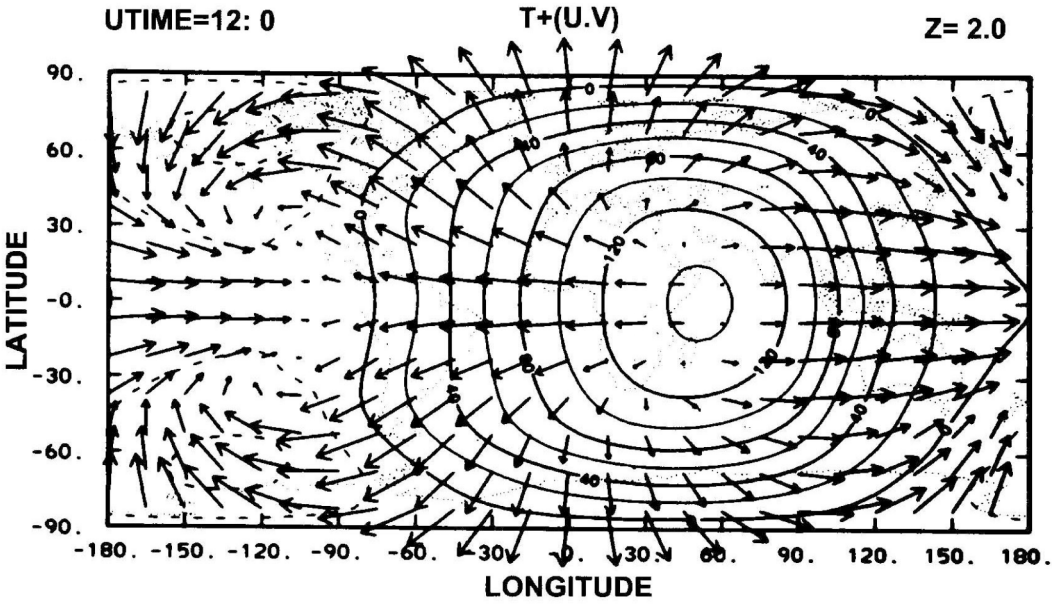

(a)

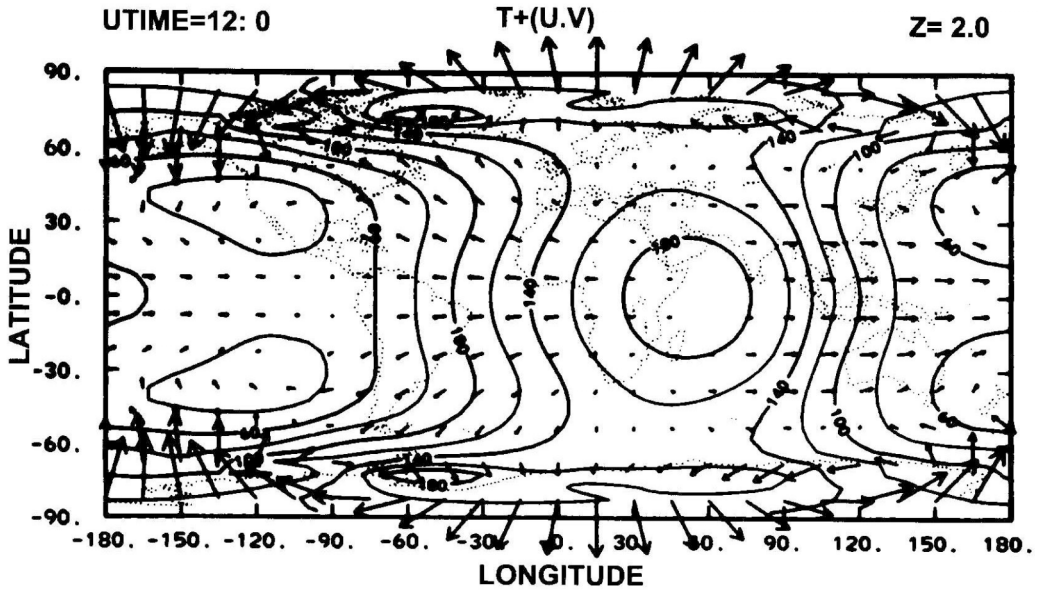

(b)

～300km altitude
(a) 100m/s maximum
(b) 336m/s maximum
60kV cross-tail potential

Circulation from GCM Model

Geomagnetic Activity

Quiet

Average

Storm

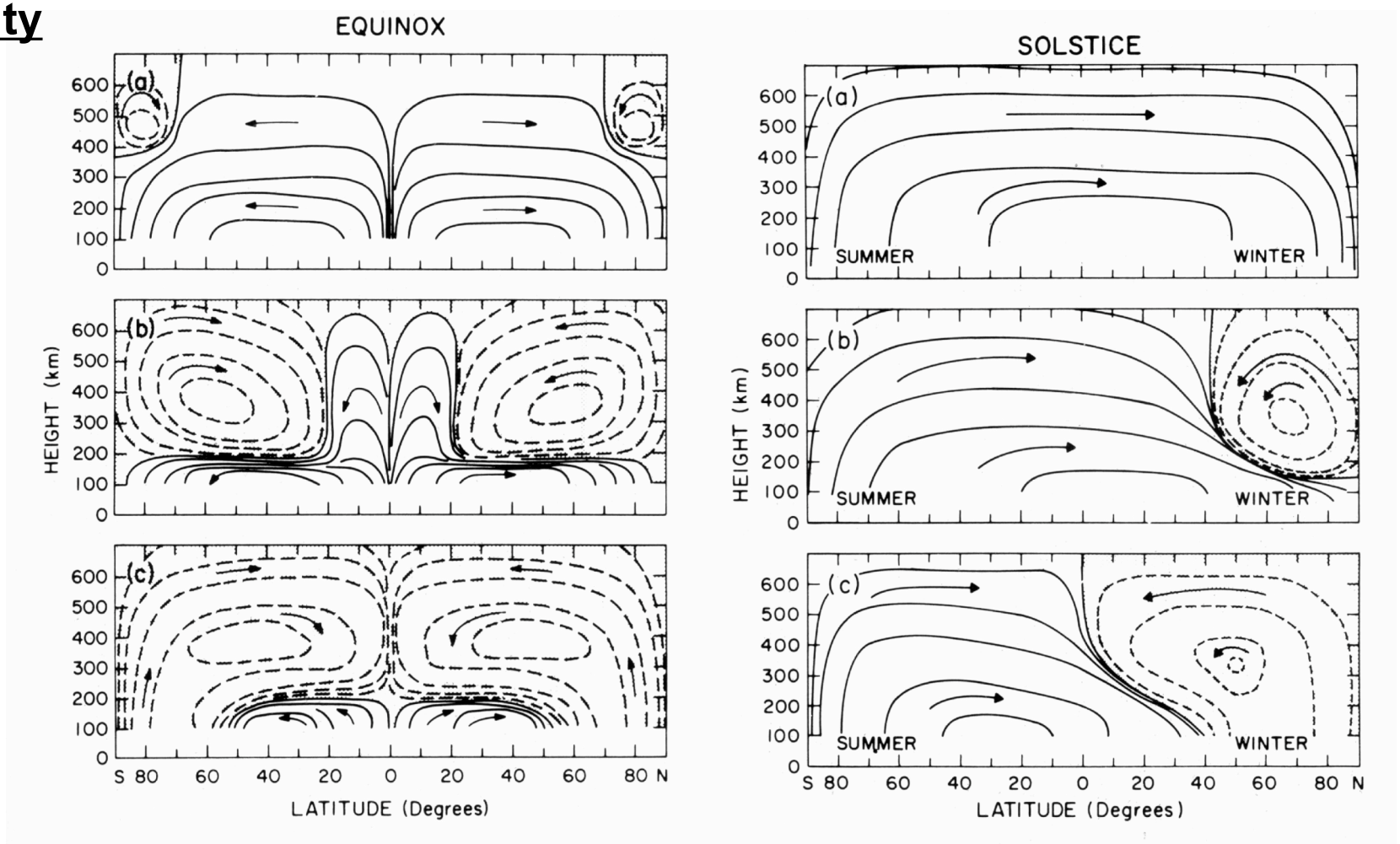

Heating/Ion Drag in Thermosphere

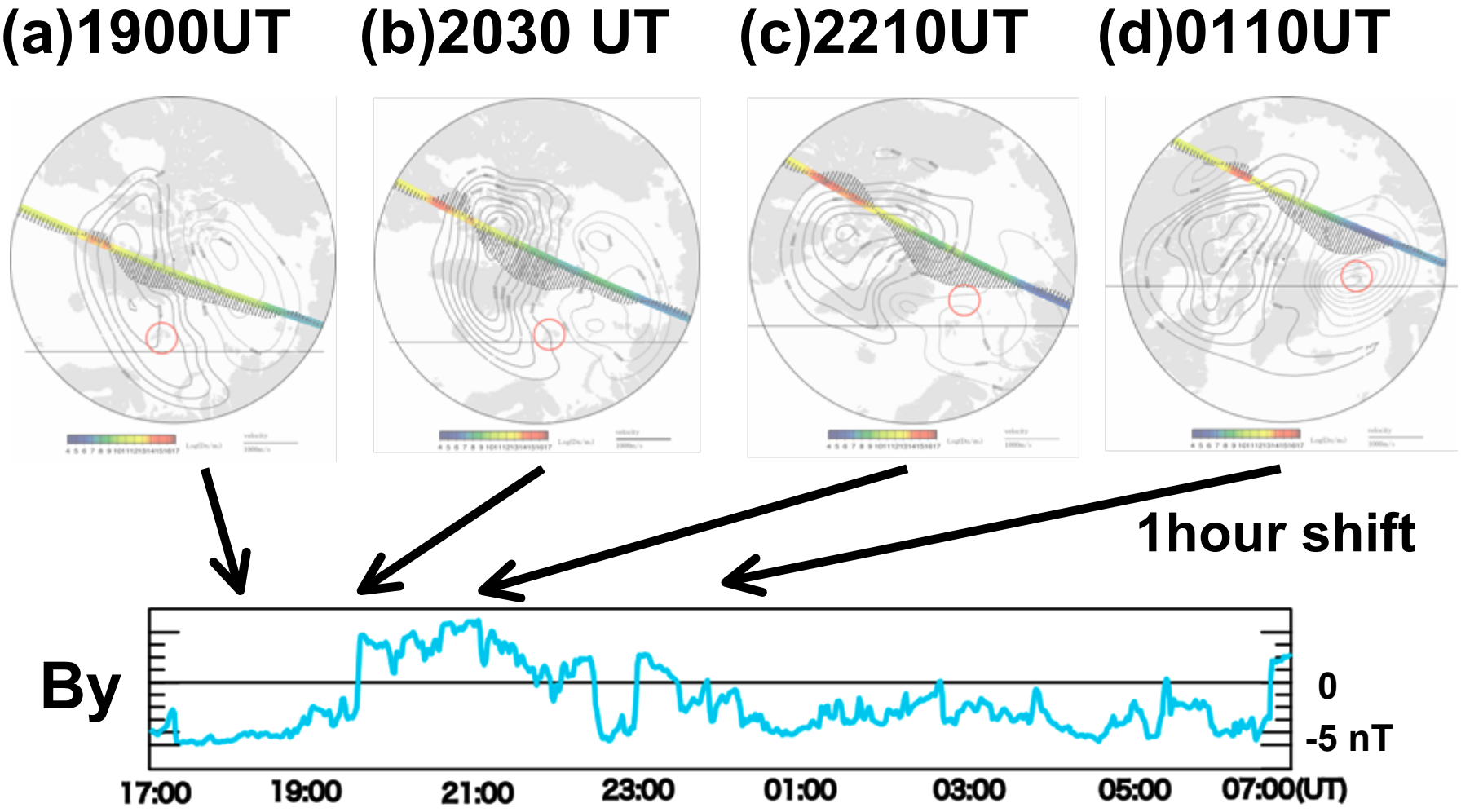

April 16, 2002

Travelling Atmospheric Disturbances (TADs)

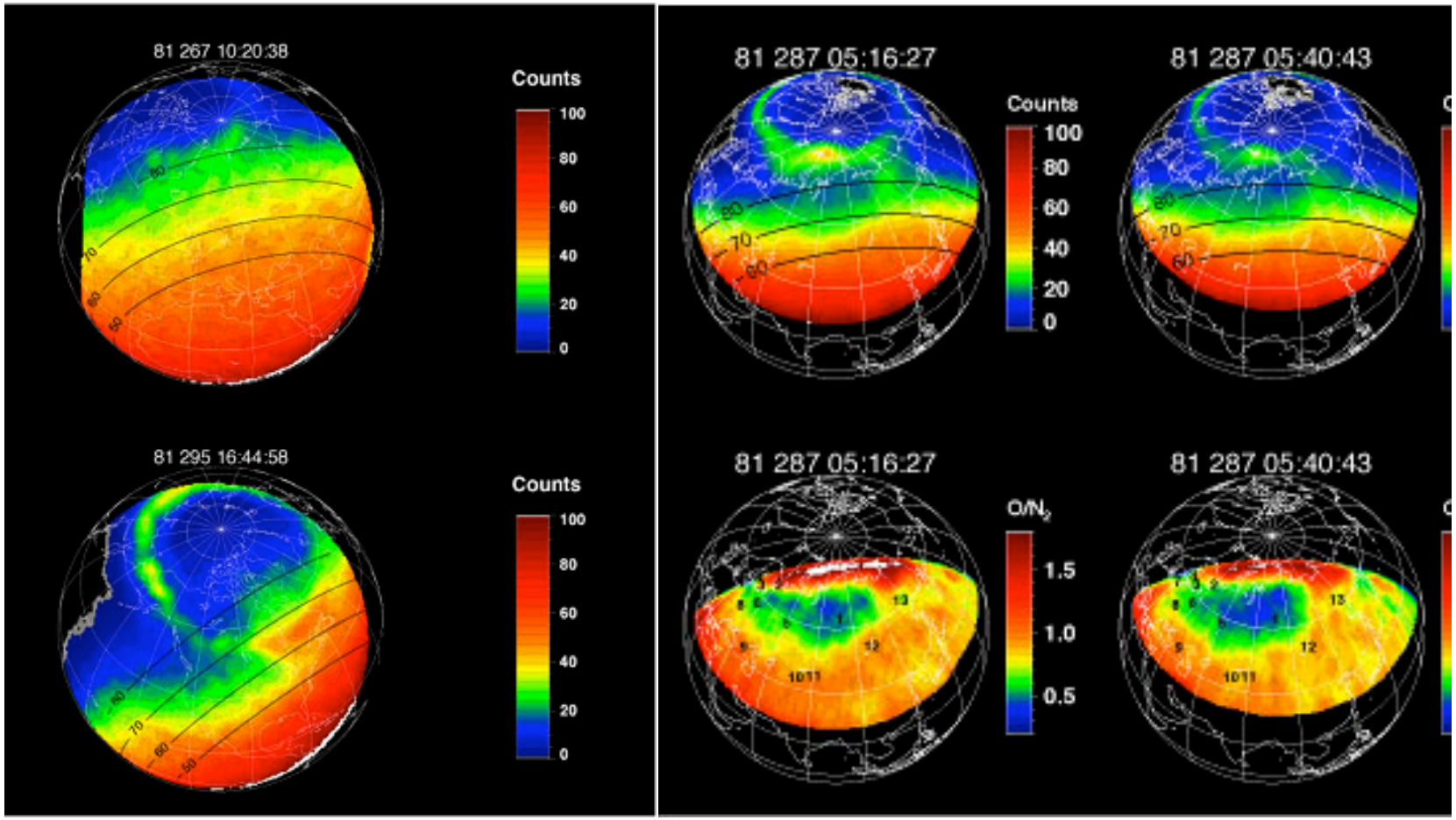

DE1, 130nm large scale Acoustic Gravity Waves (AGWs)

Negative Ionospheric Storm

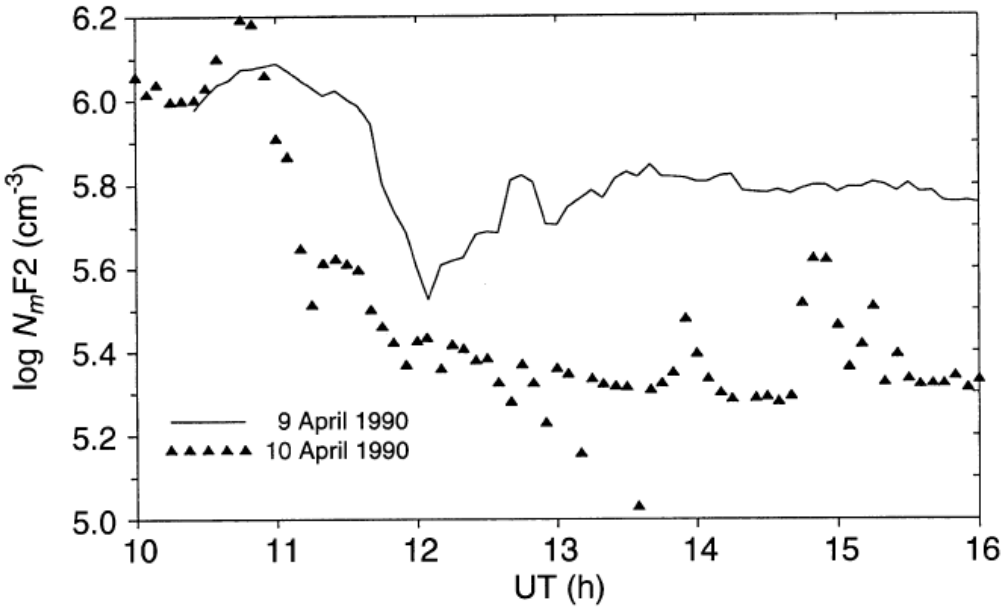

EISCAT

A. Mikhailov, K. Schlegel
Ann. Geophysicae, 1998

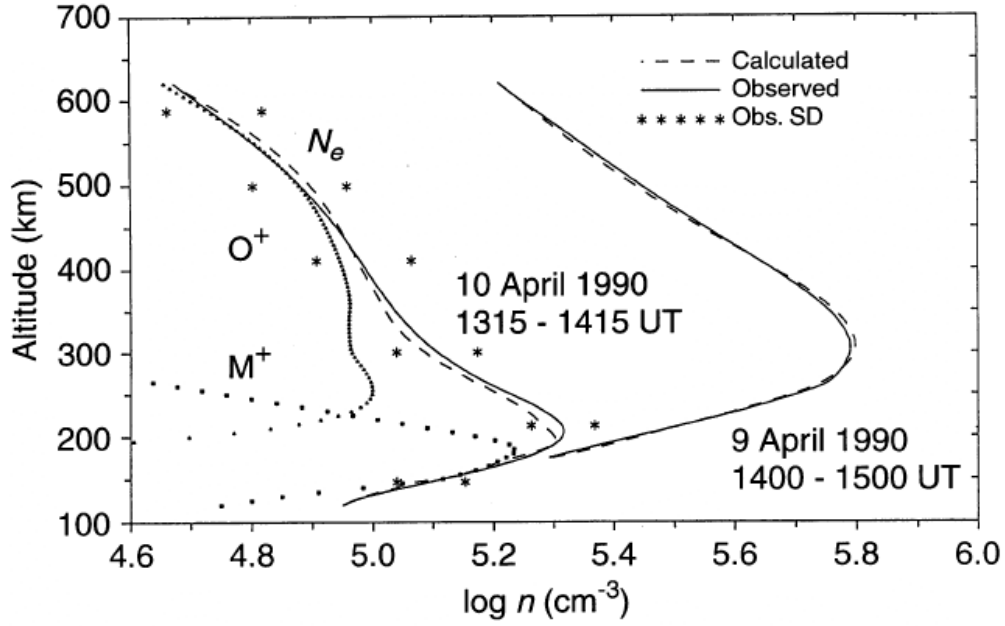

O/N_2比の減少
による電子密度減少

Positive Ionospheric Storm

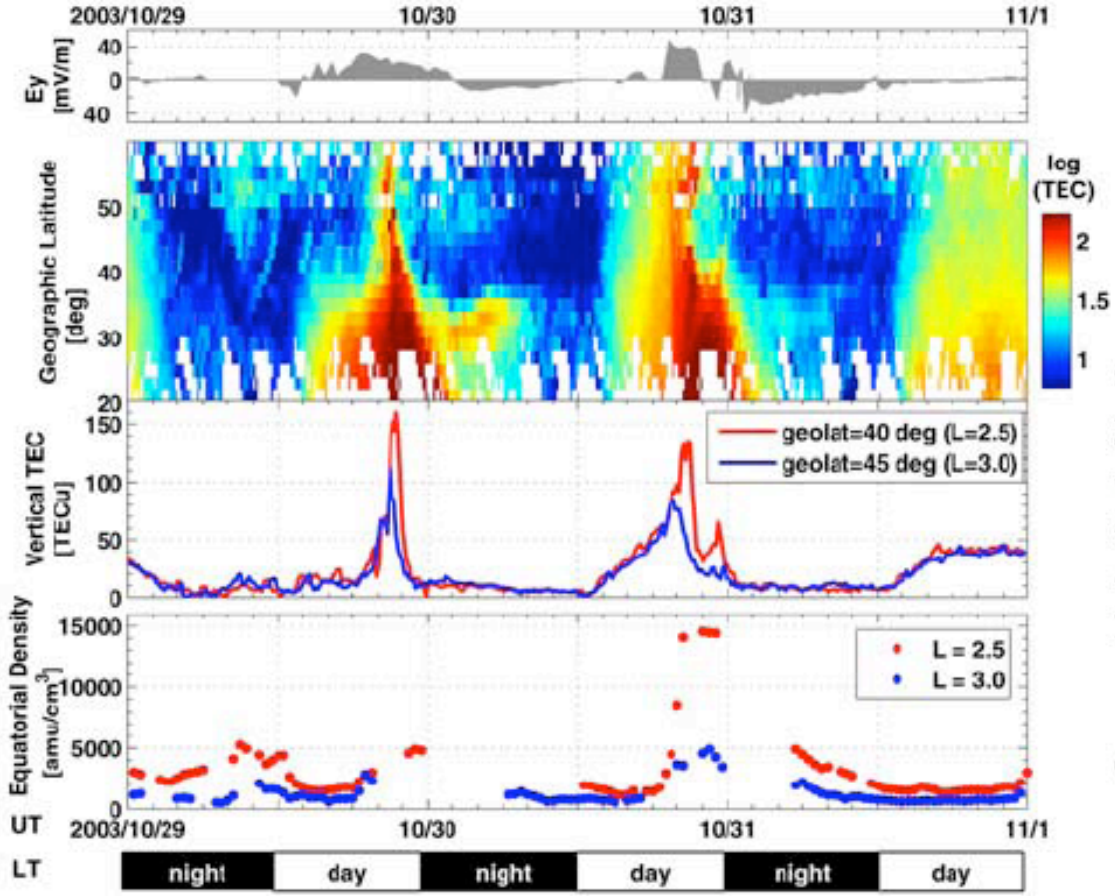

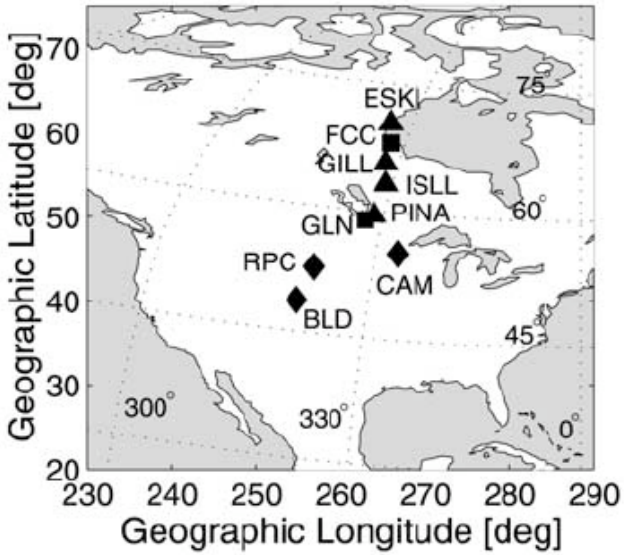

Figure 3. (From top to bottom) The IMF E_y (eastward), the vertical total electron content (TEC) along the 255° geographic longitude, the same vertical TEC values at L = 2.5 and 3.0, and the equatorial plasma density at approximately 255° geographic longitude and at the same L-values inferred by field line resonance measurements.

P. J. Chi et al, 2005

Large Scale Travelling Ionospheric Disturbances (LSTIDs)

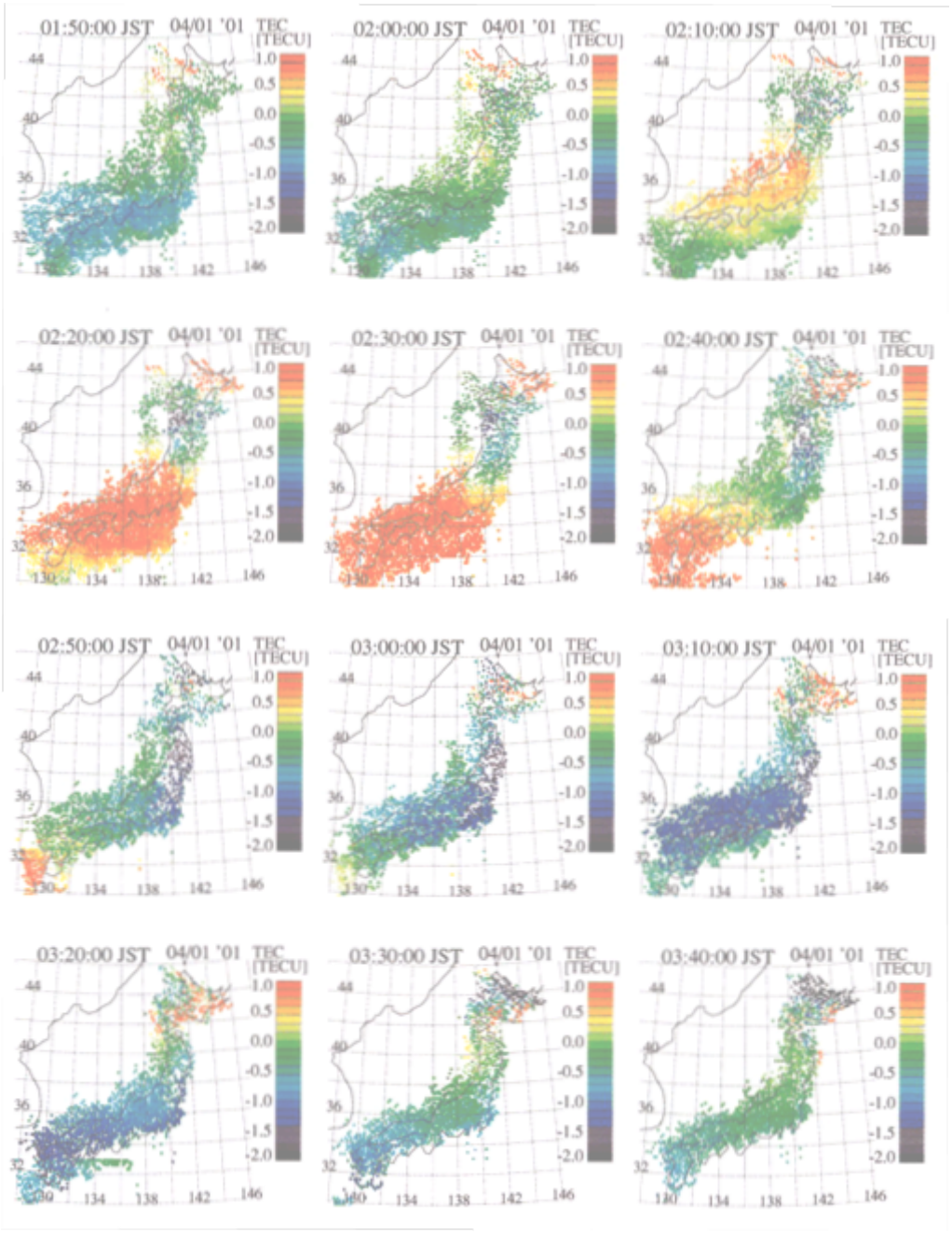

~400m/s

Ionosphere/Thermosphere/Plasmasphere

1. 磁気圏プラズマ供給源としての電離層
2. 熱圏嵐と電離圏嵐
3. プラズマ不安定

Plasma Density Irregularity

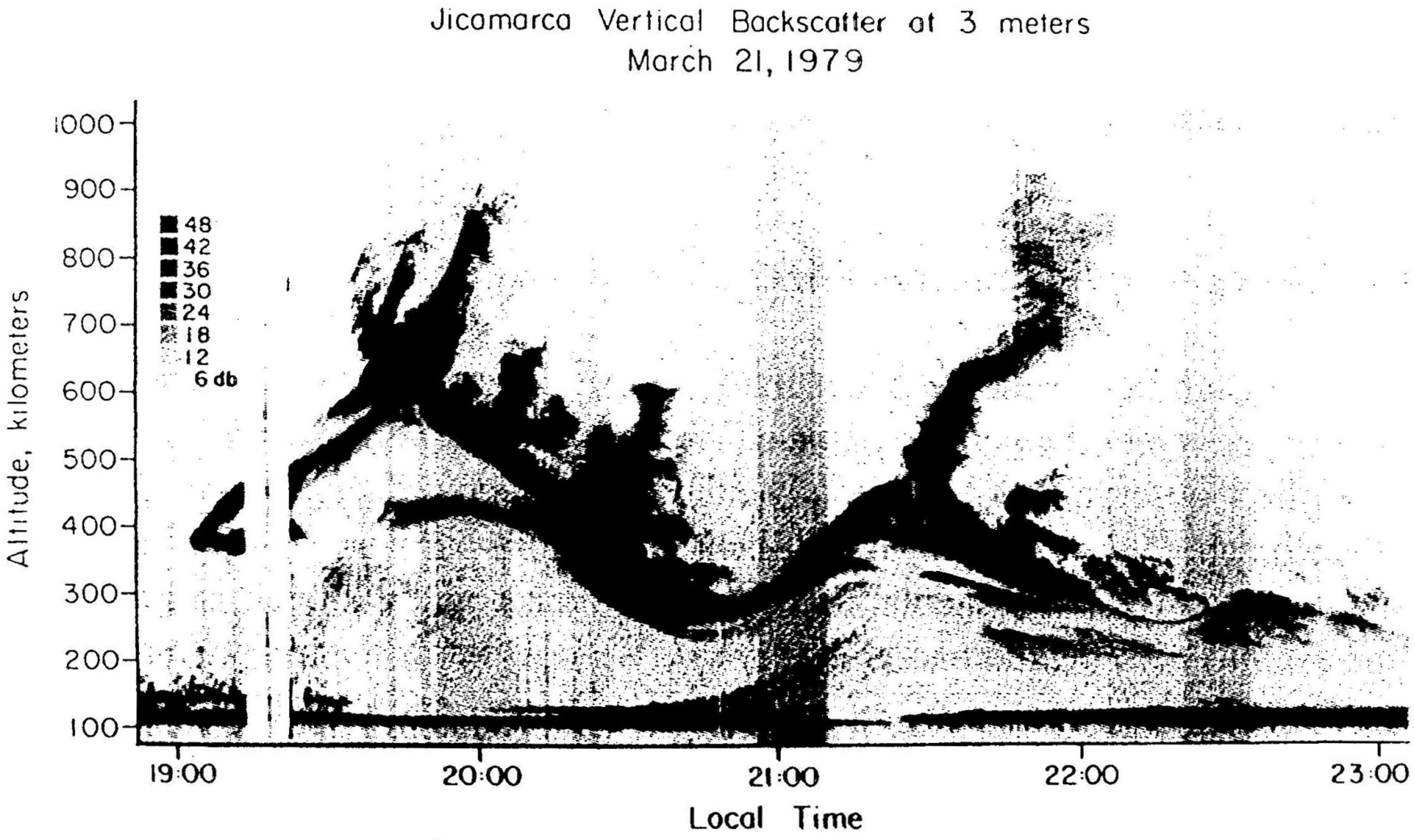

Fig. 4.1. Range–time–intensity map displaying the backscatter power at 3-m wavelengths measured at Jicamarca, Peru. The gray scale is decibels above the thermal noise level. [After Kelley *et al.* (1981). Reproduced with permission of the American Geophysical Union.]

Plasma Bubble

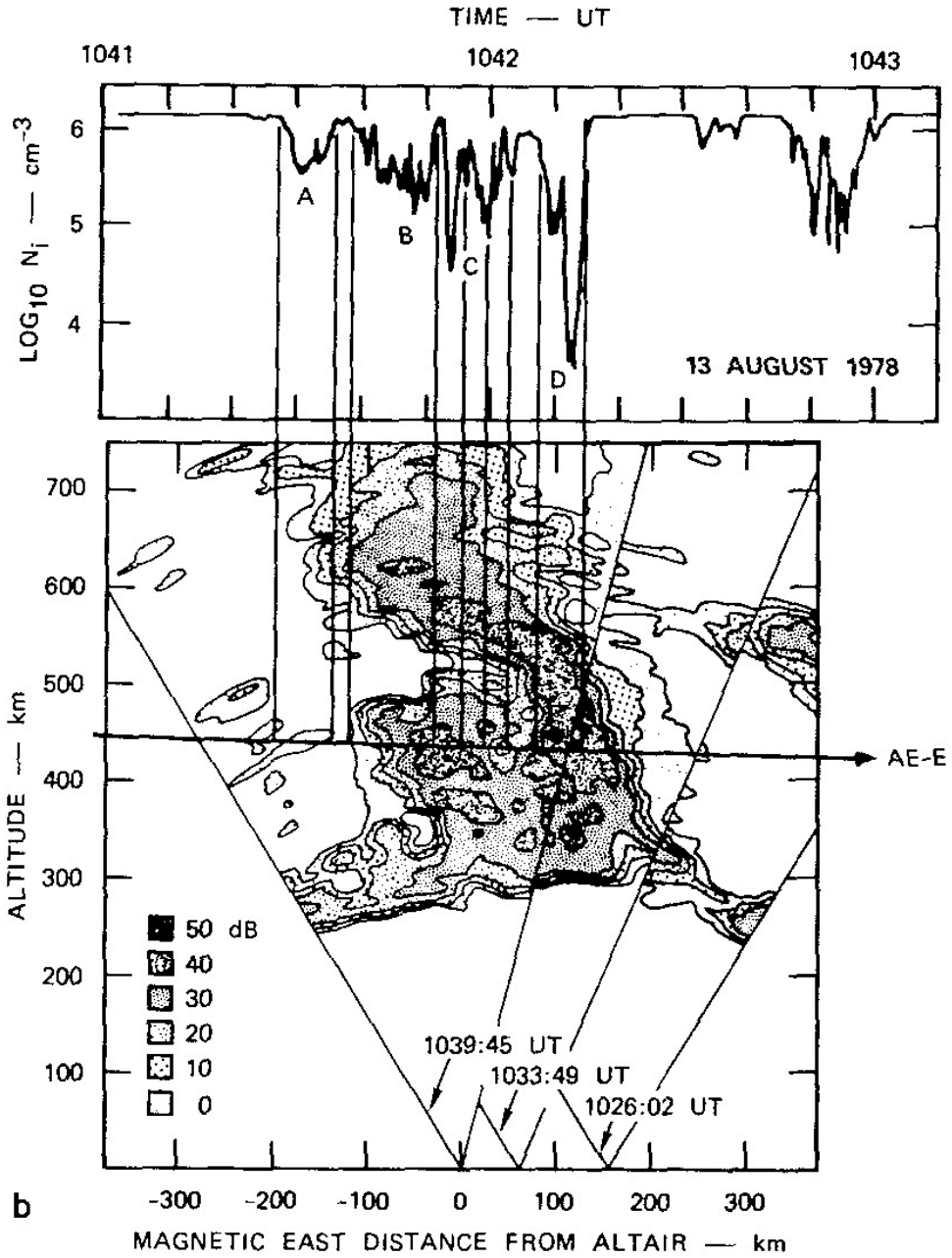

Sintilation associated with Plasmas Bubble

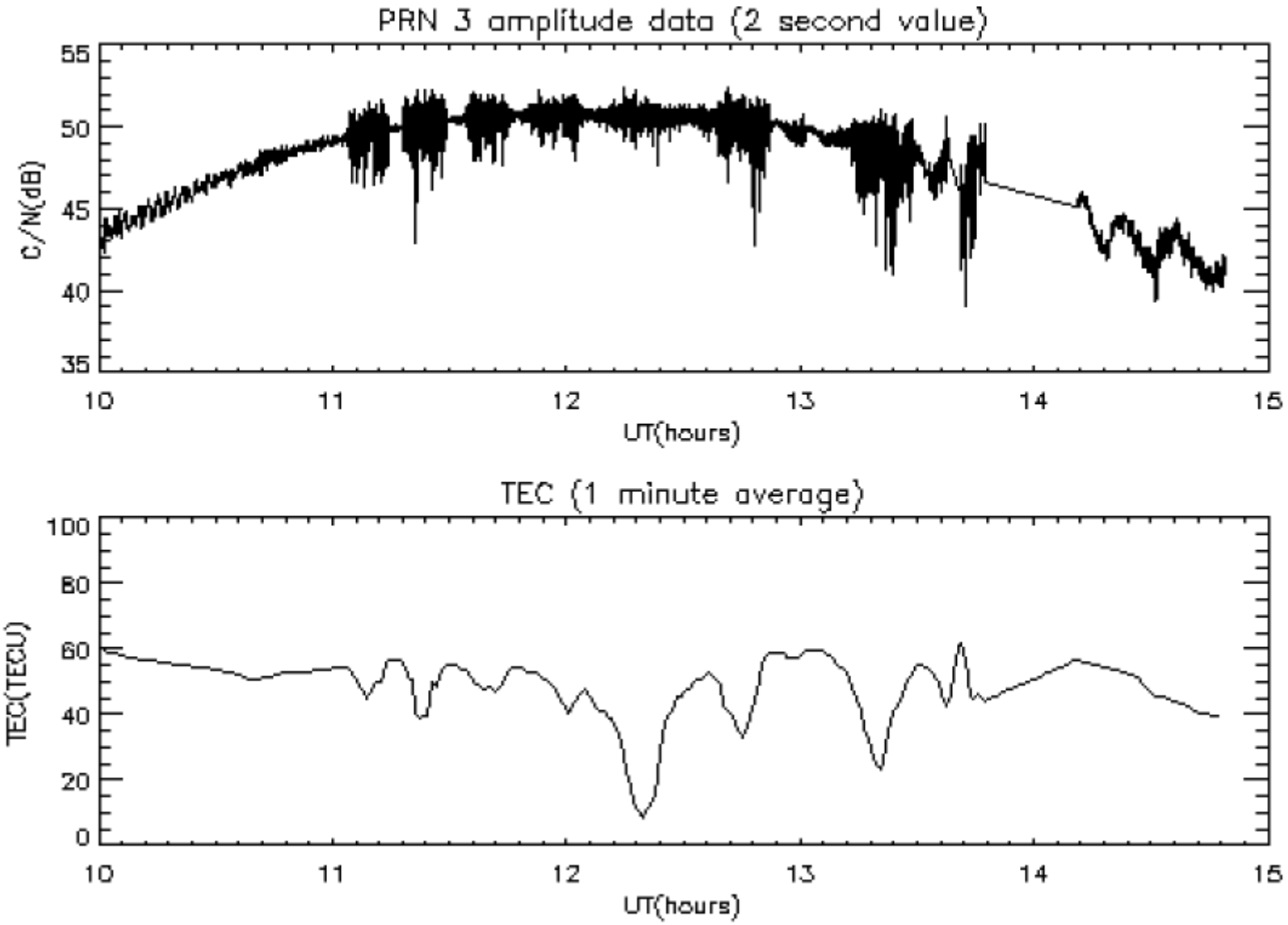

GPS L1(1.57542GHz) signal at Vanimo on 20 September 1999

Plasma Density Irregularity Spectrum

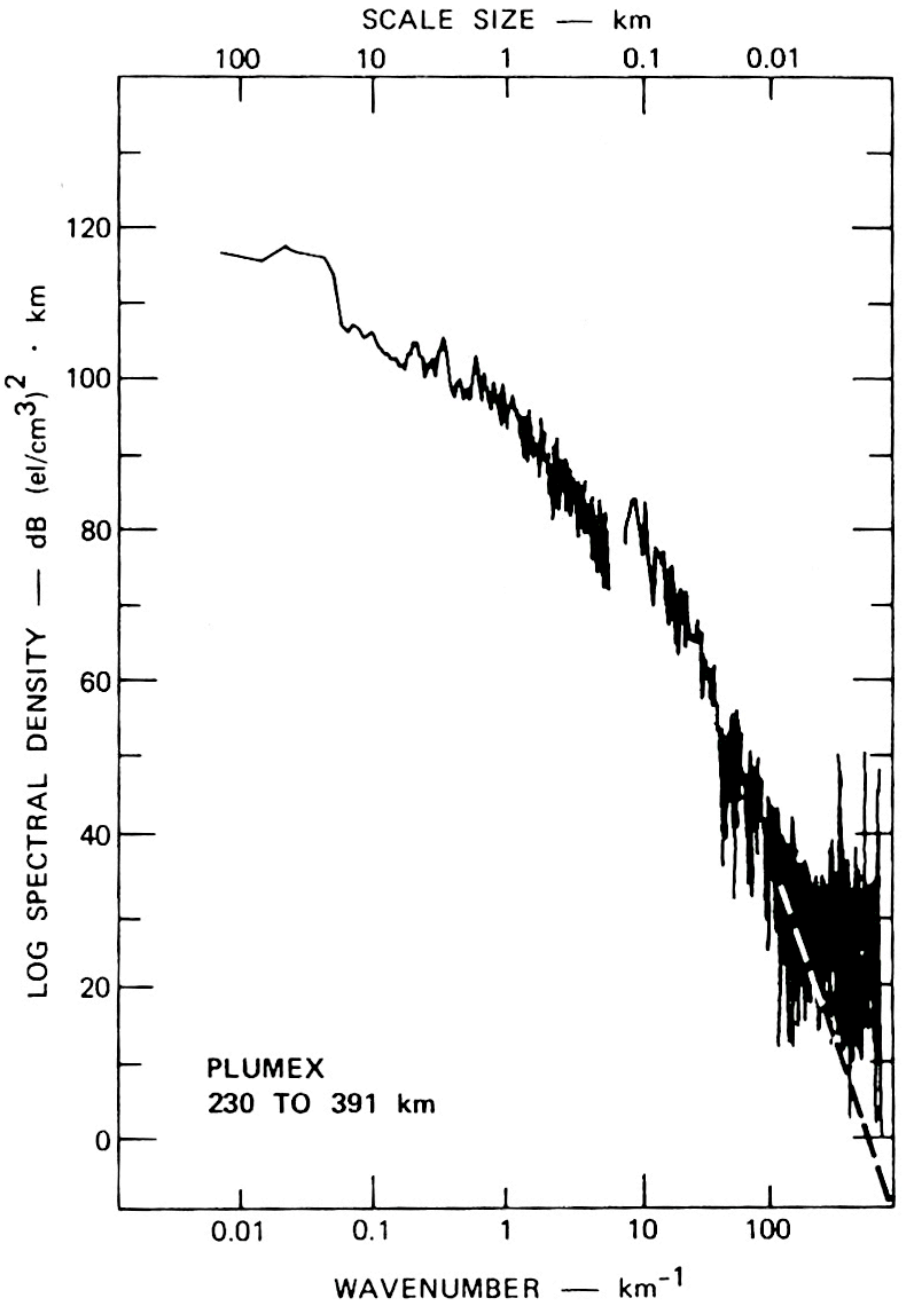

Rayleigh-Tayler Instability

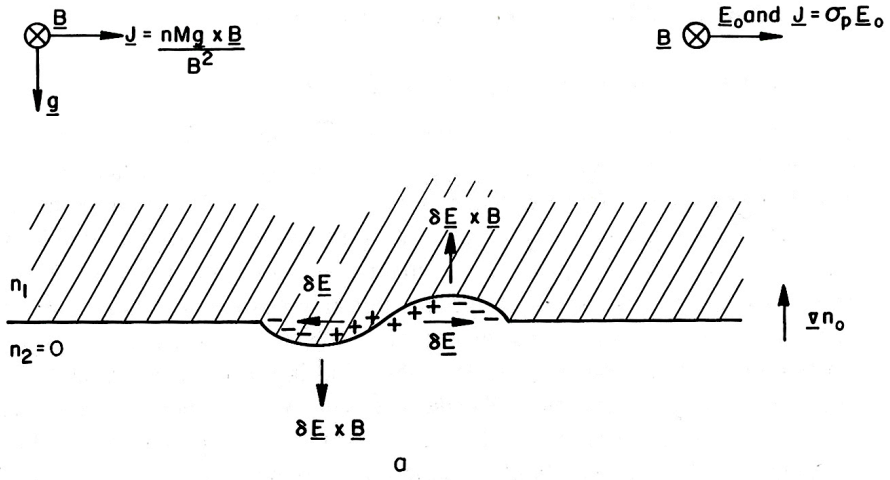

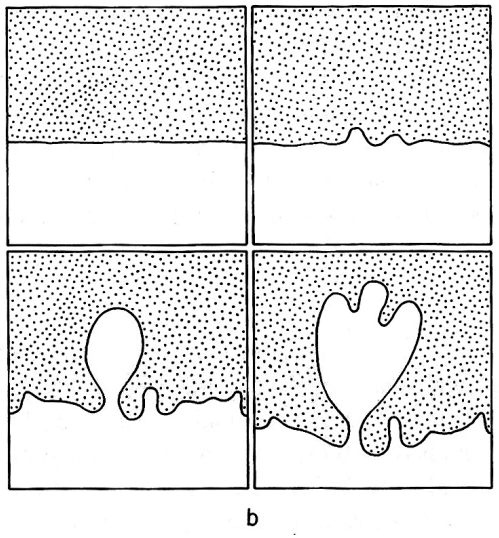

$$\frac{\partial n}{\partial t} + \nabla(n\mathbf{v}) = 0, \quad \nabla \cdot \mathbf{J} = 0$$

$$\gamma = \left(\frac{g}{\nu_{in}} + \frac{E_x}{B} + \frac{\nu_{in} u_{nx}}{\Omega_i} \right) \frac{1}{n_0} \frac{\partial n_0}{\partial z}$$

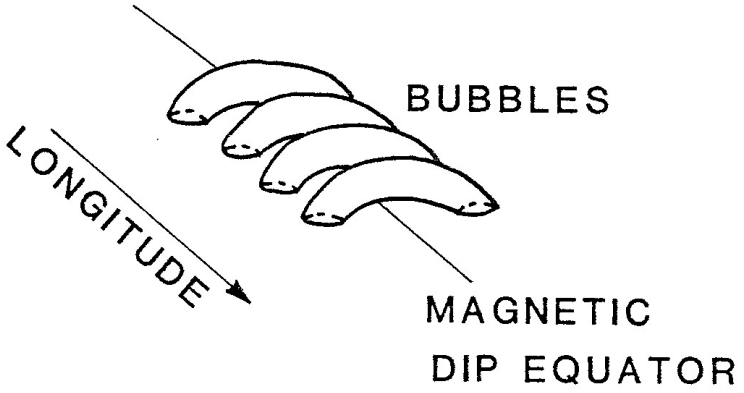

Simulation of Plasma Bubble

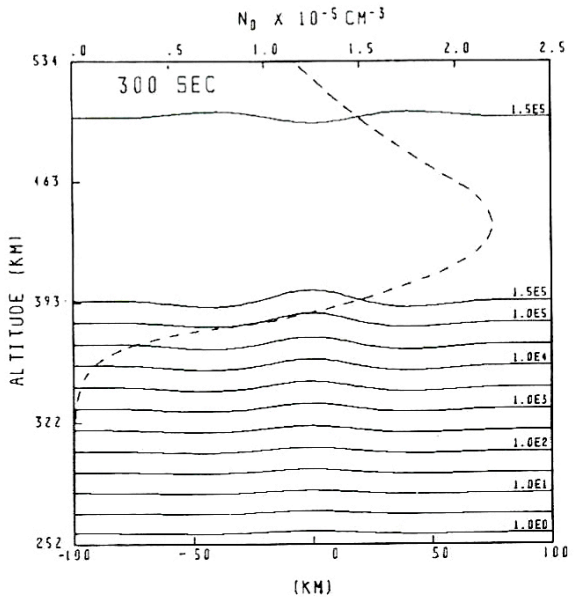

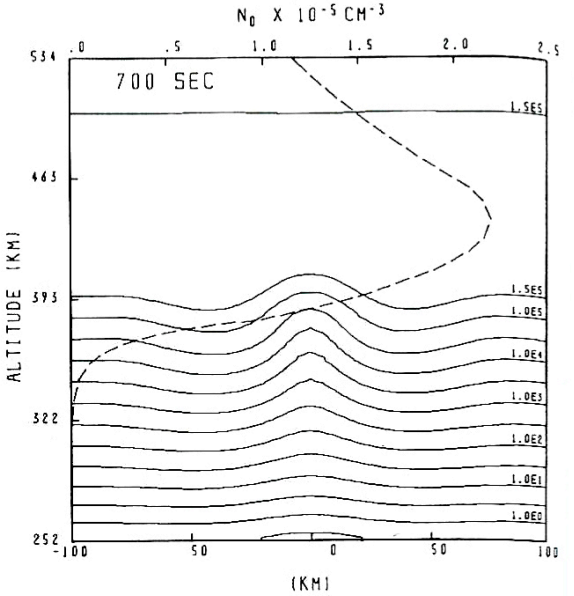

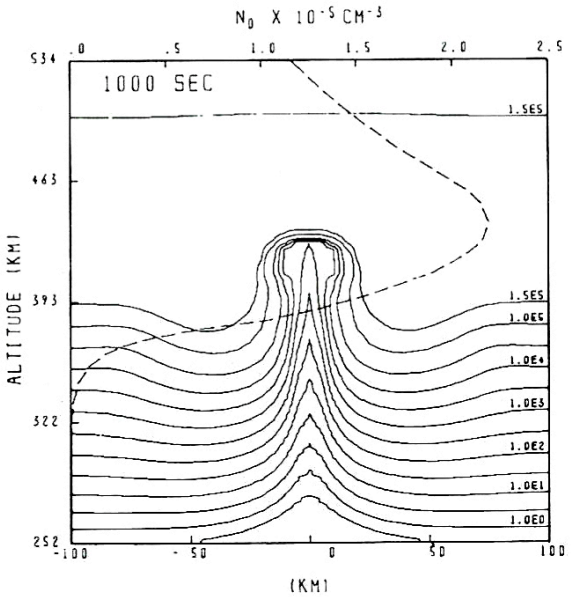

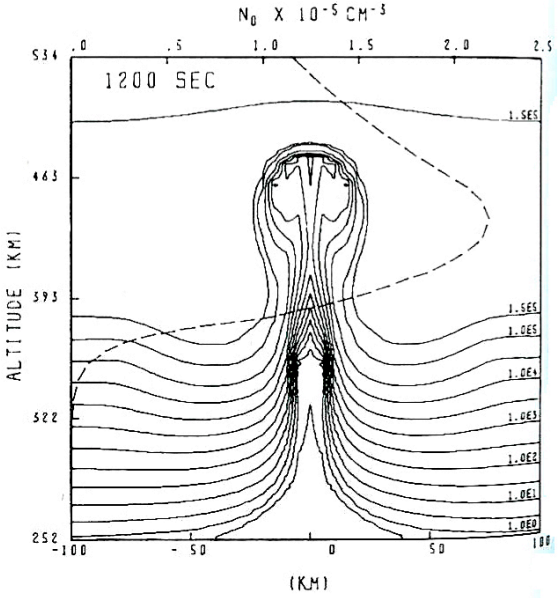

Generation of Plasma Bubble

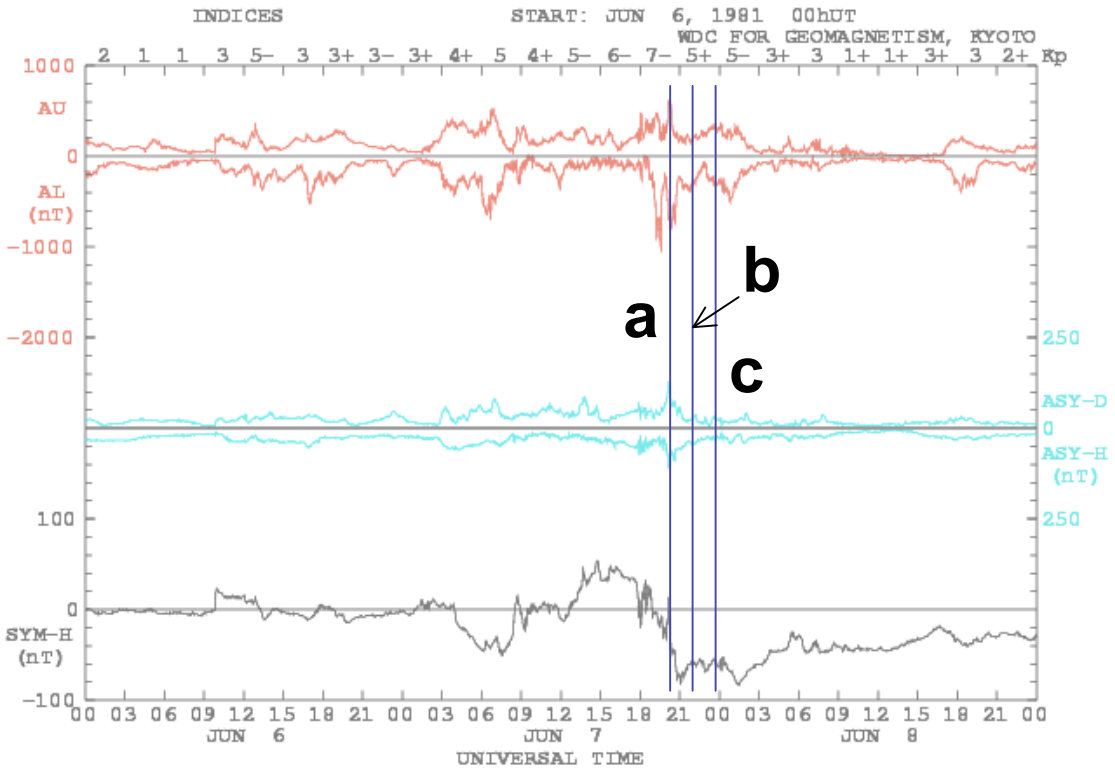

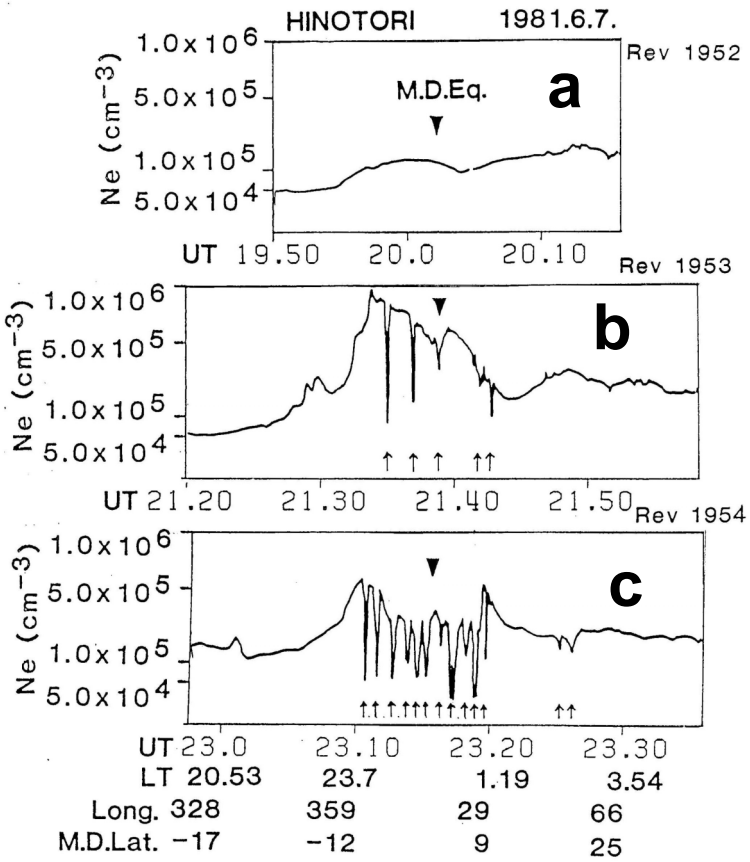

?Large Scale Circulation → Disturbance Dynamo → Eastward Electric Field → Plasma Bubble

?Direct Penetration of Electric Field

Equatorial Anomaly

（赤道異常：プラズマ密度の増加）

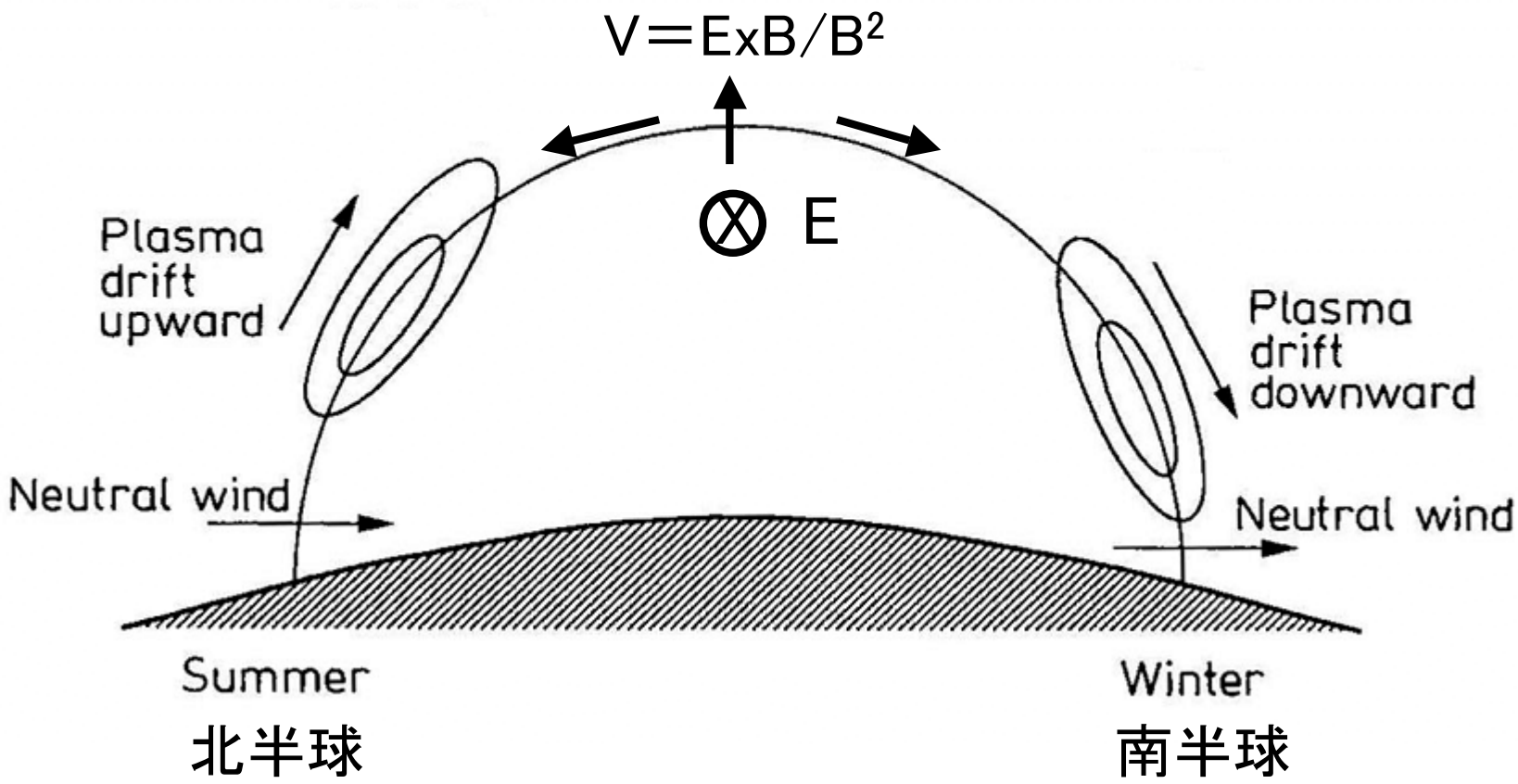

Ionosphere/Thermosphere/Plasmasphere

During Magnetic Storm

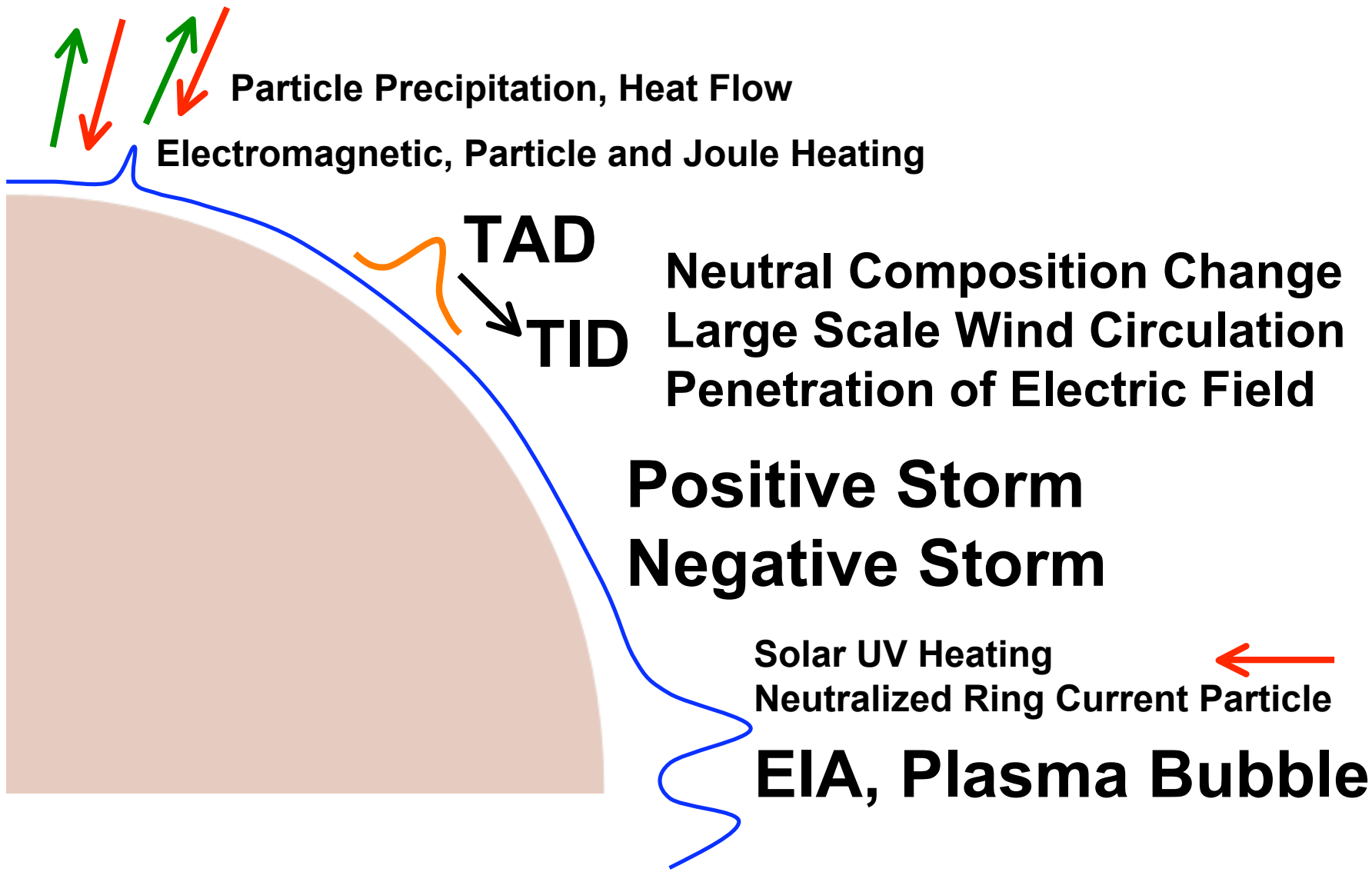

The Earth’s Nighttime Equatorial Anomaly Crests as Seen in 1356 Å Light - Photographed from the Moon

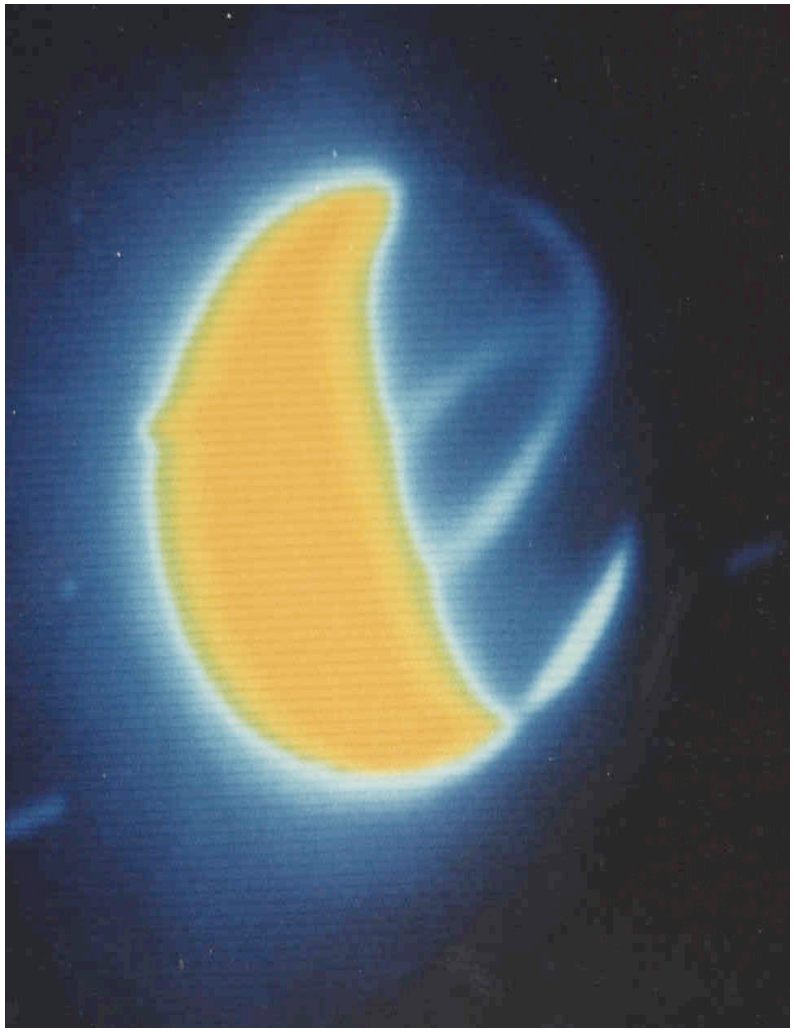

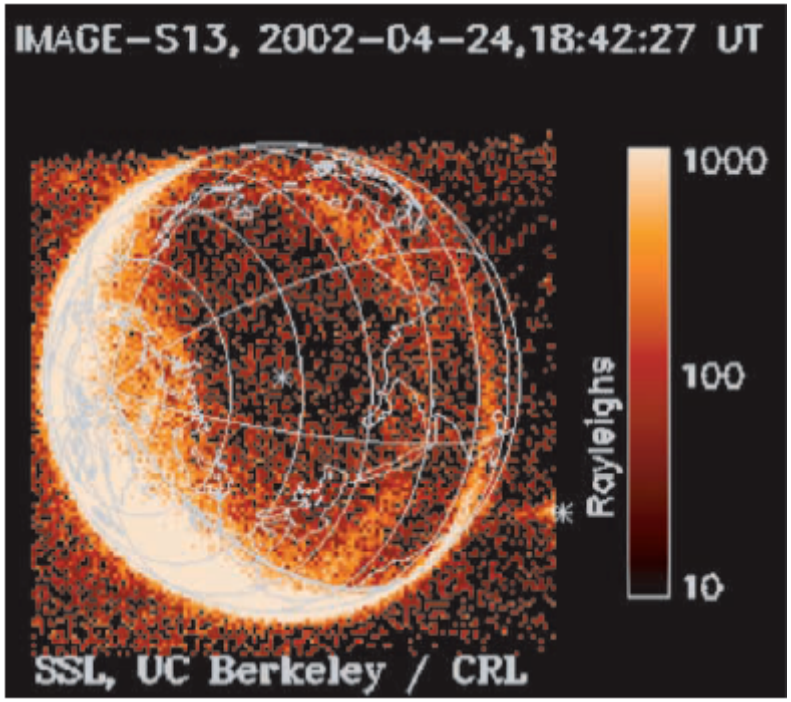

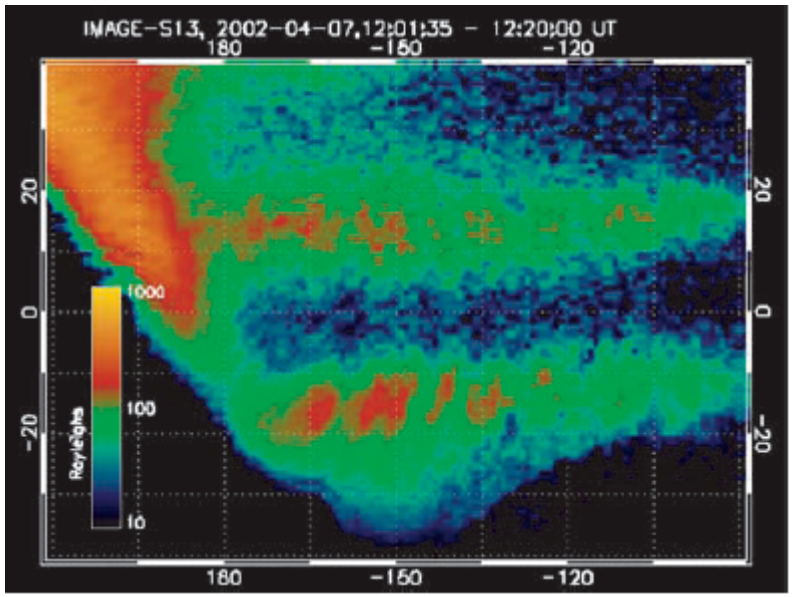

The structure may be due to the plasma density perturbations generated by acoustic gravity waves through amplification by the spatial resonance and the Rayleigh-Taylor (R-T) instability.

ダイナモ電場の生成
－ E-Region Dynamo －

$$\mathbf{J} \approx en\left(\mathbf{u}_n - \frac{\mathbf{E}\times\mathbf{B}}{B^2}\right)$$

$$\nabla\cdot\mathbf{J} = \nabla\cdot\left(en\left(\mathbf{u}_n - \frac{\mathbf{E}\times\mathbf{B}}{B^2}\right)\right) = 0$$

$$\therefore \mathbf{E} = -\mathbf{u}_n \times \mathbf{B}$$

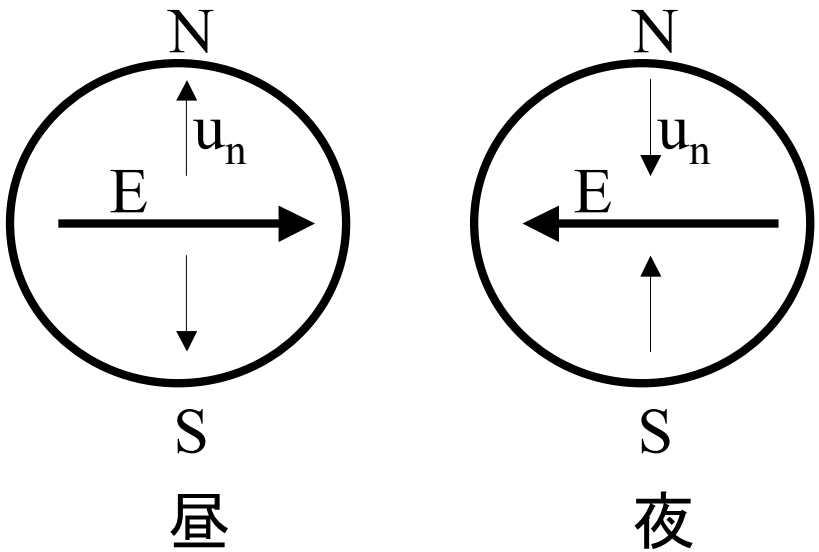

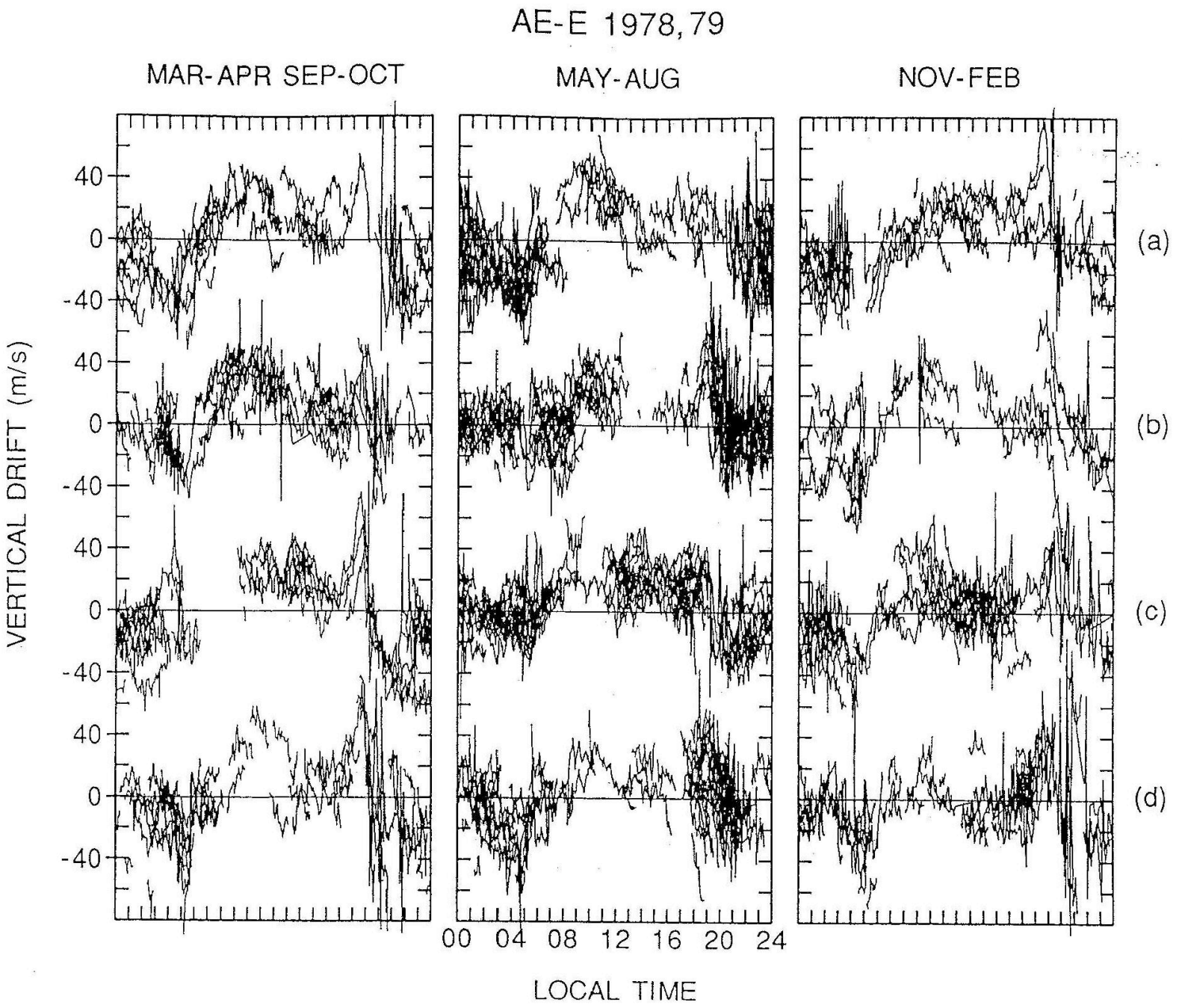
AE-E 1978,79
MAR-APR SEP-OCT
MAY-AUG
NOV-FEB
VERTICAL DRIFT (m/s)
40
0
-40
(a)
(b)
(c)
(d)
00 04 08 12 16 20 24
LOCAL TIME

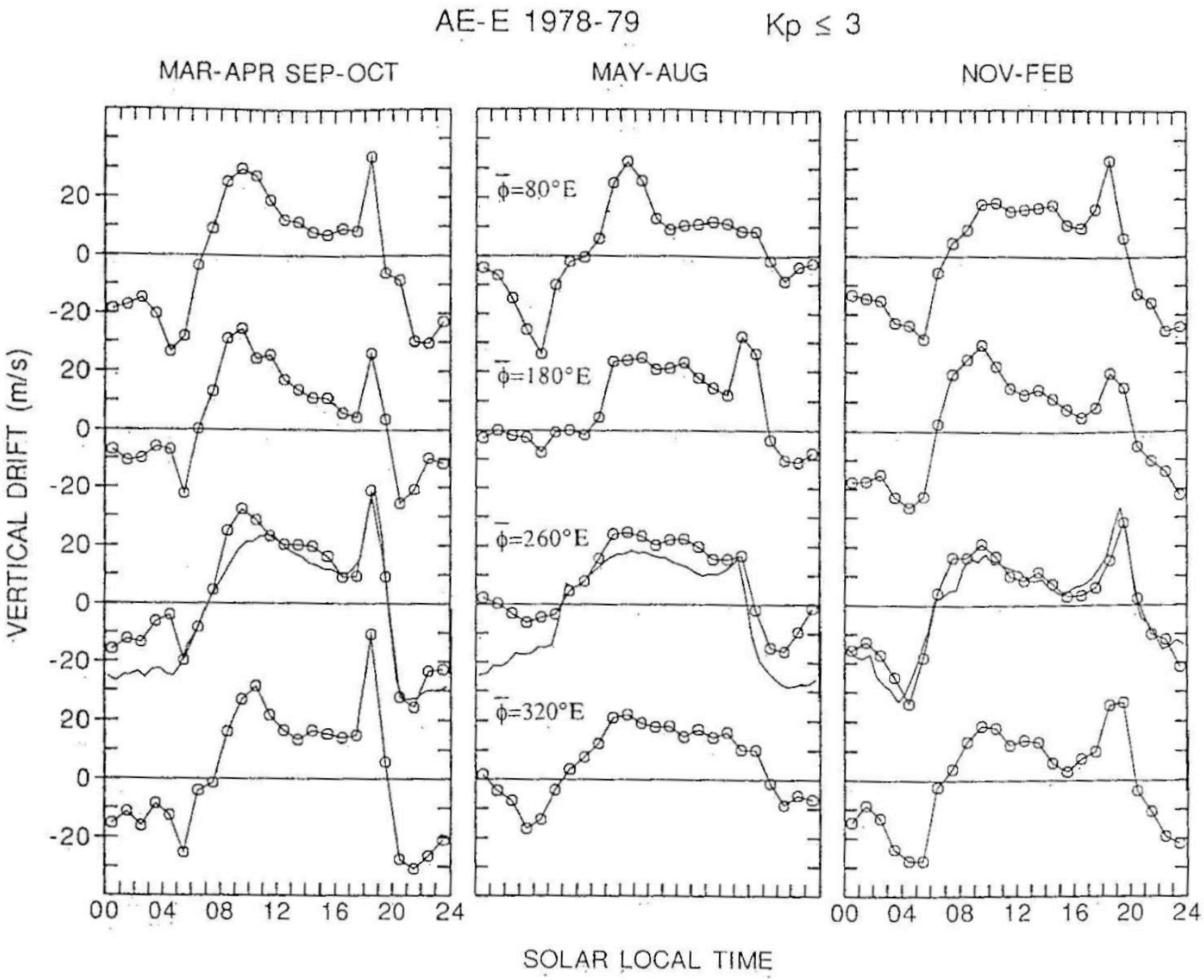
AE-E 1978-79
Kp ≤ 3
MAR-APR SEP-OCT
MAY-AUG
NOV-FEB
$\bar{\phi}$=80°E
$\bar{\phi}$=180°E
$\bar{\phi}$=260°E
$\bar{\phi}$=320°E
VERTICAL DRIFT (m/s)
20
0
-20
00 04 08 12 16 20 24
SOLAR LOCAL TIME

ダイナモ電場の生成
－ F-Region Dynamo －

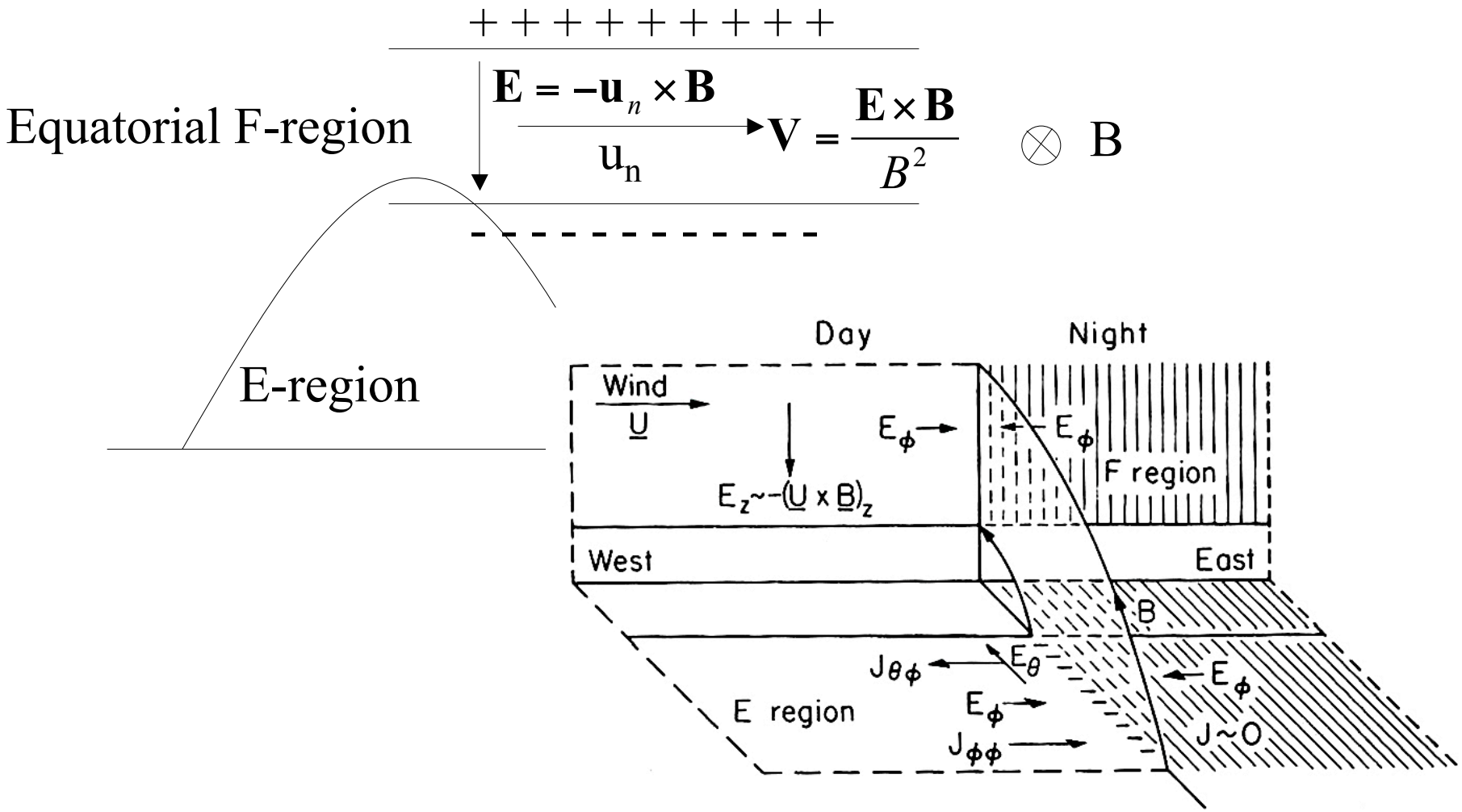

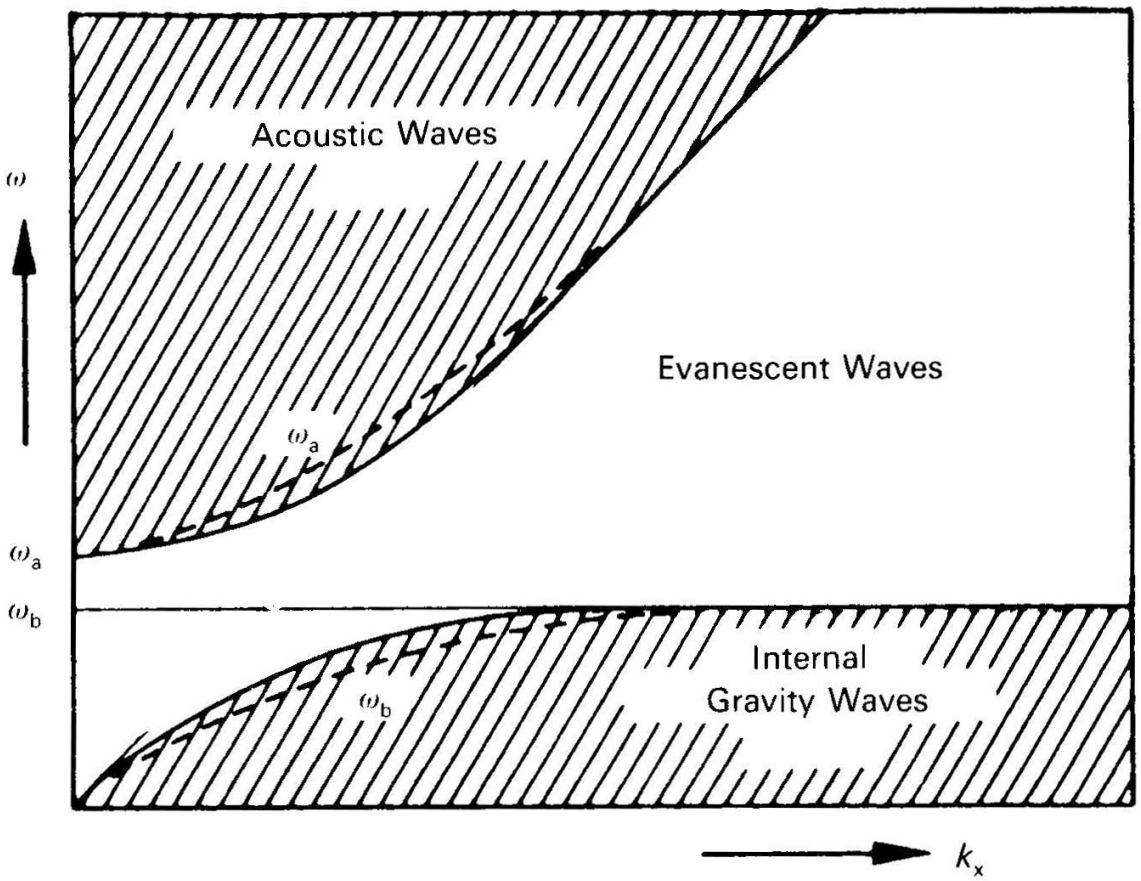

Fig. 4.23 The acoustic, evanescent, and gravity regimes of acoustic–gravity waves. The dashed lines show the effect of neglecting gravity and compressibility respectively. (After J. C. Gille, in *Winds and Turbulence in Stratosphere, Mesosphere and Ionosphere*, (ed. Rawer). North-Holland, 1968. Elsevier Science Publishers)

2001年3月29日

可視光

X線

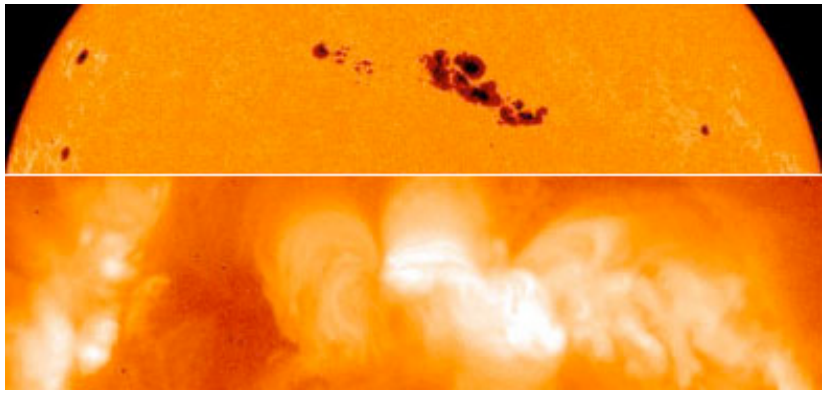

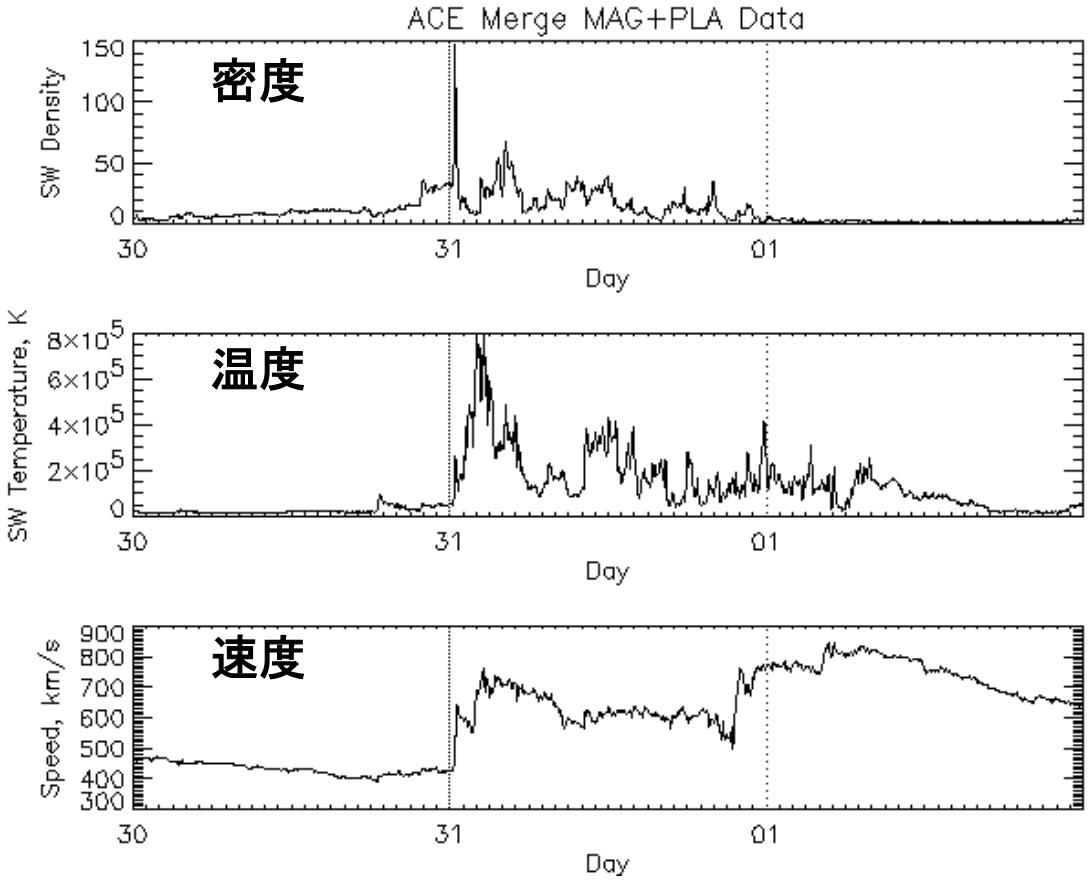

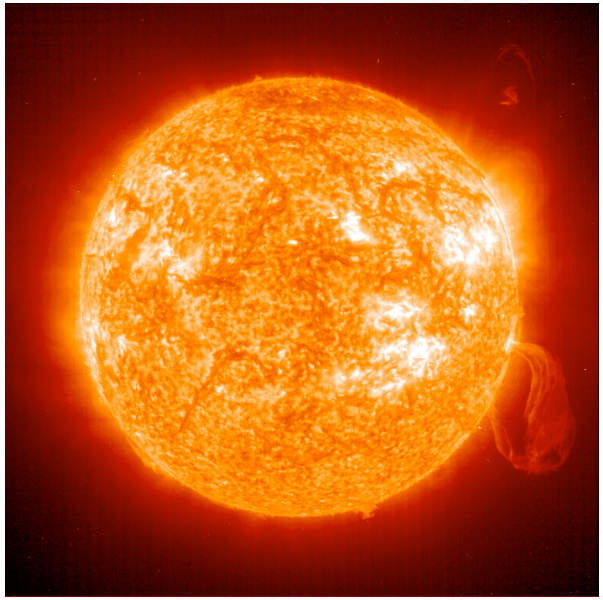

2001年3月1日

March 29 - April 1, 2001 Aurora

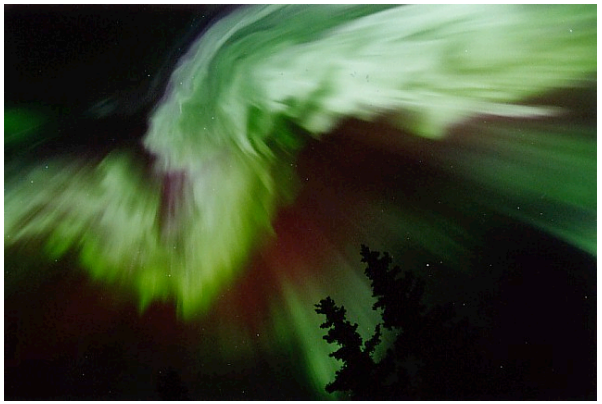

Alaska

Payson, Arizona

Rikubetsu

Dunedin, New Zealand

Nice, France

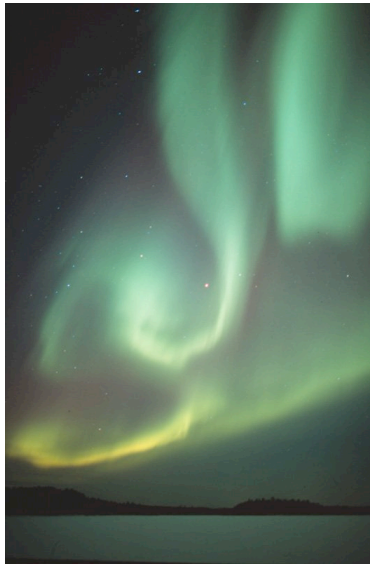

Oulu, Finland

2001年3月，4月

- 3月22日太陽東端に活動領域が発生．地球直径の22倍の大きさ
- コロナからプラズマ放出（10^{22}J，広島原子爆弾10^{13}J）
- 地球に到達し，各地でオーロラ発生
- 通信障害が発生（デリンジャー現象が約６時間継続）通信衛星，航空機（アジアー北米間で25航空機のトラブル），船舶，放送局で通信できない状態が発生
- 電力送信障害が発生
- NASAは火星探査機（Odyssey）の打ち上げを延期
- 宇宙空間の放射線レベルが10倍以上に増加．飛翔中のスペースシャトルに注意警告

2003年10月

「こだま」の姿勢制御系に異常.「マーズオデッセイ」の観測器で異常. 月探査衛星「SMART-1」のエンジンが自動停止.「みどりII」の機能停止.「チャンドラX線天文衛星」が1日間観測を停止. 宇宙ステーションの乗組員が避難.

2000年7月

太陽からの高エネルギー粒子により, 1時間で「SOHO」衛星の太陽電池パネルの性能が1年分低下. X線天文衛星「あすか」の姿勢に乱れが生じ観測運用を断念.

1998年5月

ドイツの衛星が故障, 米国と日本の衛星が通信障害, 4イリジウム衛星が故障(4500万人のユーザが影響を受けた).

1997年1月

米国の通信衛星が故障.

1994年

カナダの2衛星が故障. NHK放送が突然停止.

1989年3月

多くの衛星が故障. カナダで電力送電線に誘導電流が流れ変圧器の焼損, 9時間に及ぶ大停電が発生し, 600万人が被害を受ける. 事故後の対策に数10億円を要した.

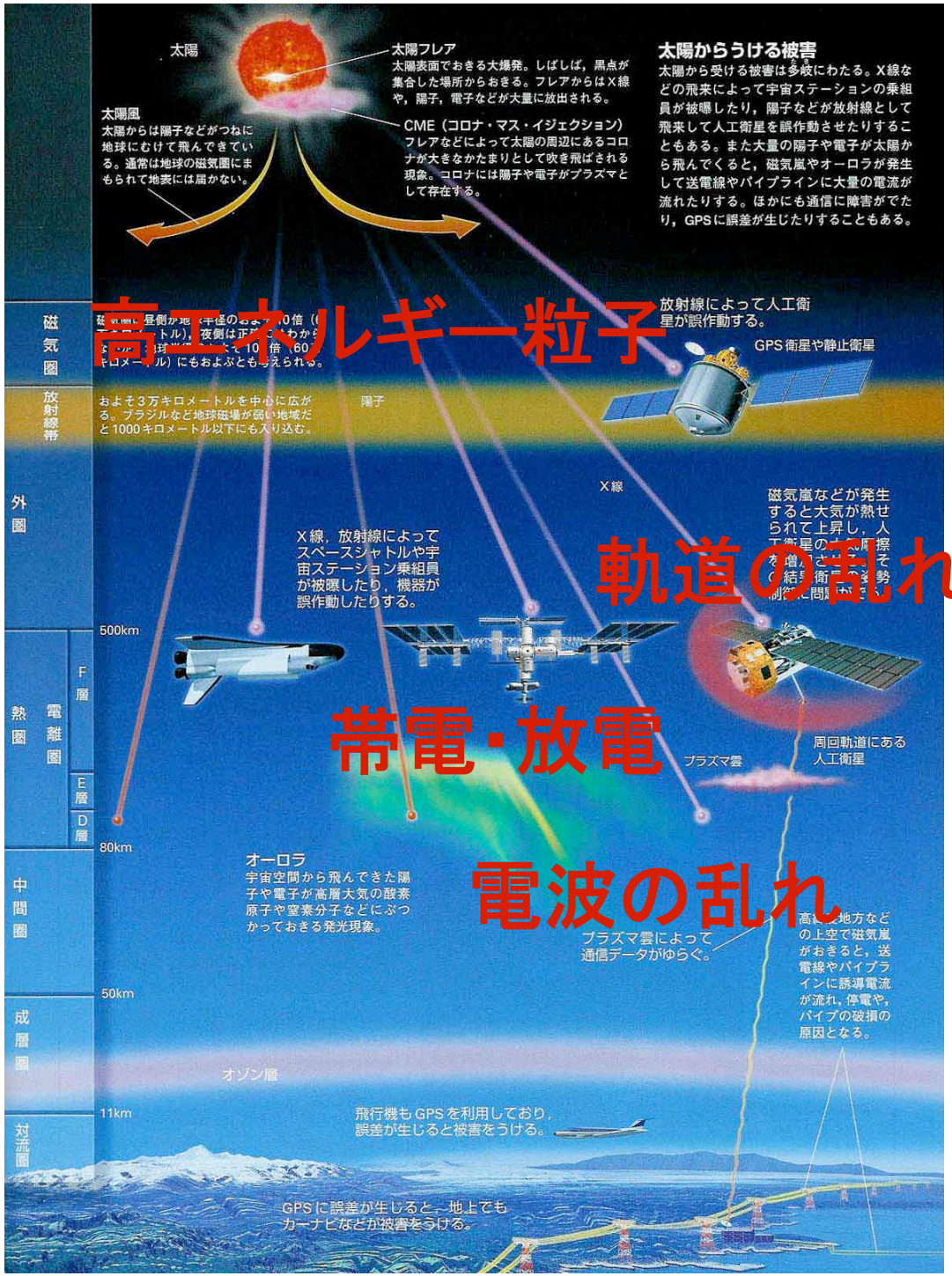

高度

40000km

10000km

500km

100km

地上

Disturbance Main Phase

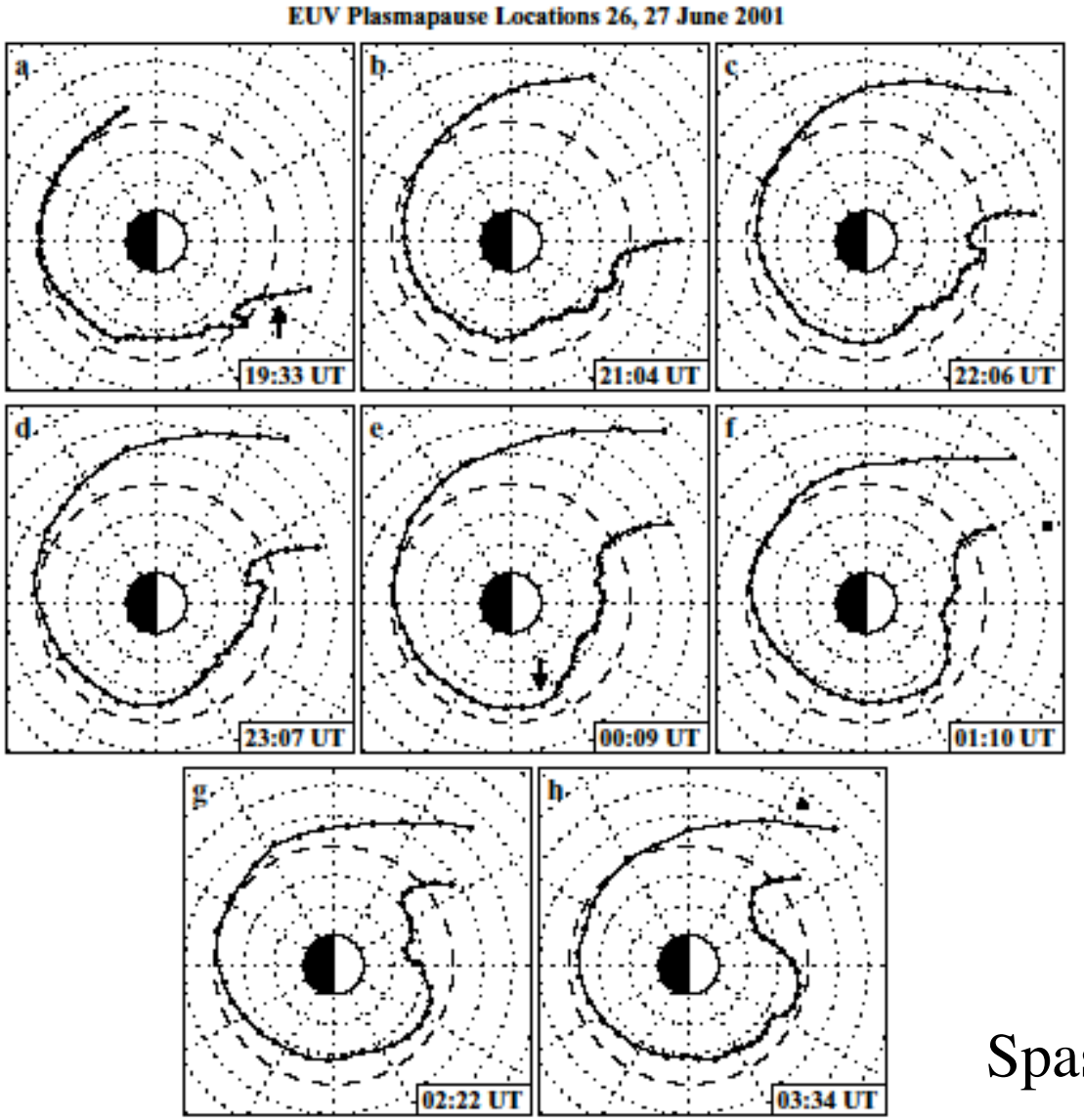

Spasojevic et al.

Recovery Phase

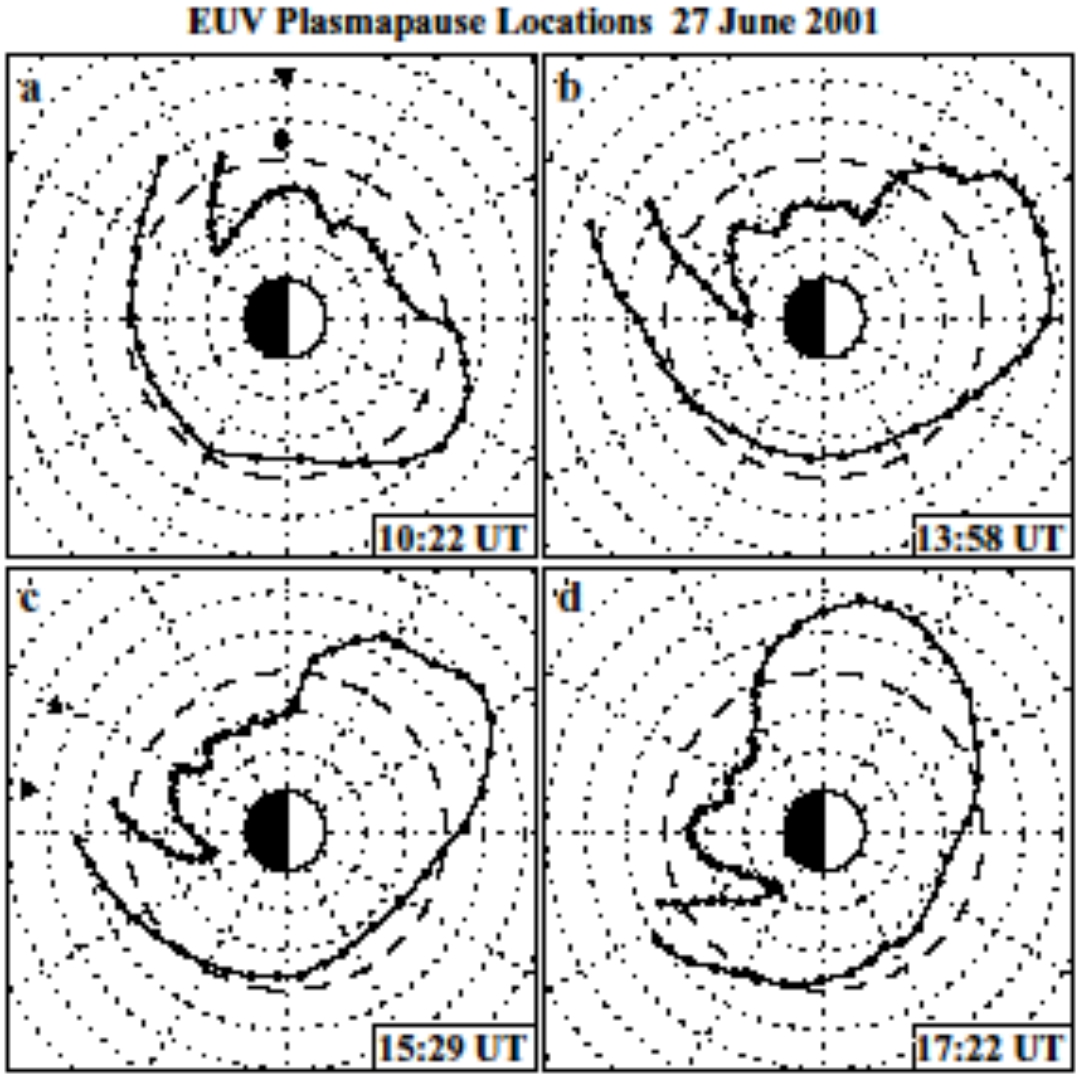

Spasojevic et al.

Plasmaspheric Ion Composition Profiles

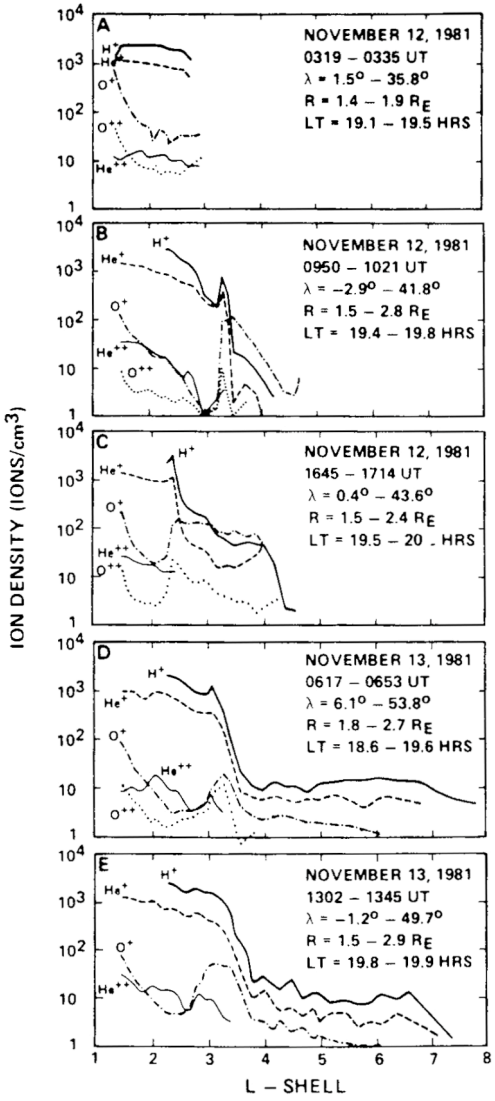

O^+ ion density reaches values comparable to the H^+ density in the region L=3-4. (Horwitz et al., 1984)

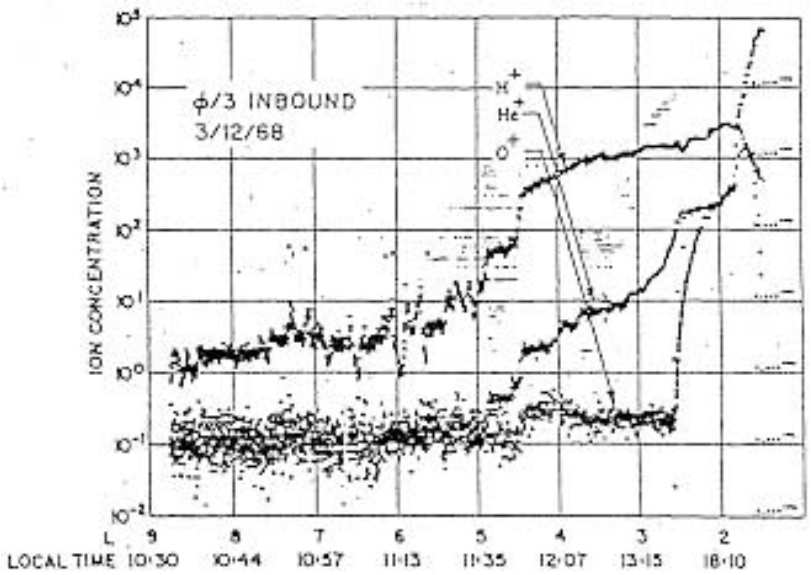

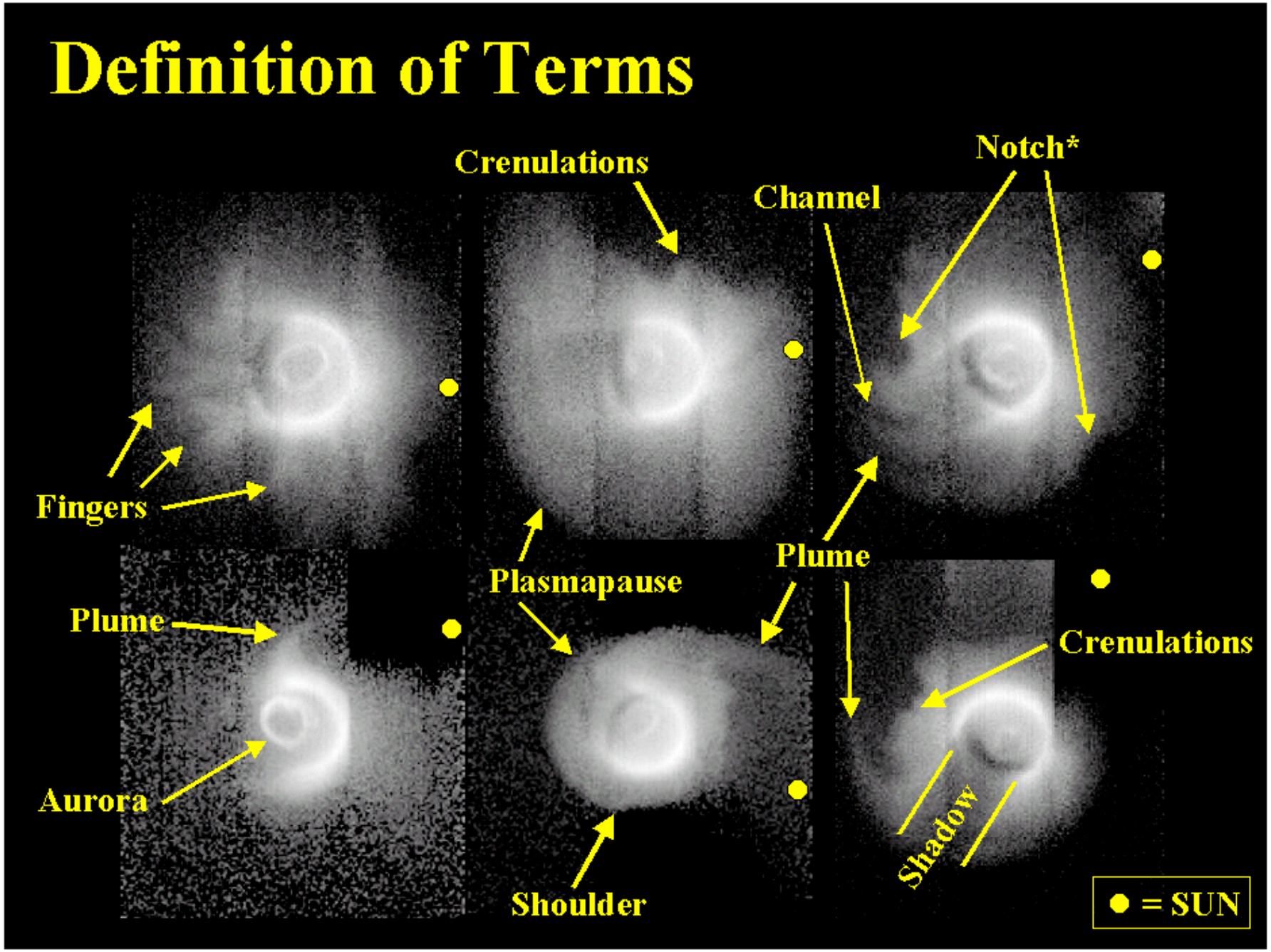
Definition of Terms
Crenulations
Notch*
Channel
Fingers
Plasmapause
Plume
Plume
Crenulations
Aurora
Shadow
Shoulder
● = SUN

Brandt